J Sci Comput (2013) 55:471–497
DOI 10.1007/s10915-012-9644-1

Two-Grid *hp*-Version Discontinuous Galerkin Finite Element Methods for Second-Order Quasilinear Elliptic PDEs

Scott Congreve · Paul Houston · Thomas P. Wihler

Received: 26 May 2011 / Revised: 15 May 2012 / Accepted: 2 September 2012 /
Published online: 11 October 2012

Abstract In this article we propose a class of so-called two-grid *hp*-version discontinuous Galerkin finite element methods for the numerical solution of a second-order quasilinear elliptic boundary value problem of monotone type. The key idea in this setting is to first discretise the underlying nonlinear problem on a coarse finite element space $V(\mathcal{T}_H, \boldsymbol{P})$. The resulting 'coarse' numerical solution is then exploited to provide the necessary data needed to linearise the underlying discretisation on the finer space $V(\mathcal{T}_h, \boldsymbol{p})$; thereby, only a linear system of equations is solved on the richer space $V(\mathcal{T}_h, \boldsymbol{p})$. In this article both the *a priori* and *a posteriori* error analysis of the two-grid *hp*-version discontinuous Galerkin finite element method is developed. Moreover, we propose and implement an *hp*-adaptive two-grid algorithm, which is capable of designing both the coarse and fine finite element spaces $V(\mathcal{T}_H, \boldsymbol{P})$ and $V(\mathcal{T}_h, \boldsymbol{p})$, respectively, in an automatic fashion. Numerical experiments are presented for both two- and three-dimensional problems; in each case, we demonstrate that the CPU time required to compute the numerical solution to a given accuracy is typically less when the two-grid approach is exploited, when compared to the standard discontinuous Galerkin method.

Keywords *hp*-finite element methods · Discontinuous Galerkin methods · Adaptivity · Two-grid methods · Quasilinear PDEs

S. Congreve · P. Houston (✉)
School of Mathematical Sciences, University of Nottingham, University Park, Nottingham, NG7 2RD, UK
e-mail: Paul.Houston@nottingham.ac.uk

S. Congreve
e-mail: pmxsc@nottingham.ac.uk

T.P. Wihler
Mathematisches Institut, Universität Bern, Sidlerstrasse 5, 3012 Bern, Switzerland
e-mail: wihler@math.unibe.ch

1 Introduction

Over the past few decades, there has been a considerable renewed interest in discontinuous Galerkin finite element methods (DGFEMs) for the numerical solution of a wide range of partial differential equations; for an extensive survey of this area of research, we refer to [7]. This article is devoted to the *a priori* and *a posteriori* error analysis of the so-called two-grid variant of the *hp*-version interior penalty (IP) DGFEM for the numerical approximation of strongly monotone second-order quasilinear elliptic partial differential equations. We point out that two-grid methods were originally introduced by Xu [30–32] in the context of continuous Galerkin finite element methods; here, non-symmetric linear and nonlinear problems have been treated. For related work, we refer to the articles [3, 5, 6, 11, 19, 26, 29] and the references cited therein. In particular, we highlight the article by Bi & Ginting [6] which represents the first attempt to apply two-grid techniques in the DGFEM setting to a class of scalar second-order quasilinear elliptic PDEs, where the nonlinear diffusion coefficient μ depends on the analytical solution u, cf. below for further discussion.

The construction of a two-grid method to compute the numerical approximation of a nonlinear partial differential equation may be summarised as follows. Let X and Y be two Hilbert spaces. Further, we write $\mathcal{N}(\cdot;\cdot,\cdot) : X \times X \times Y \to \mathbb{R}$ to denote a nonlinear form, with the convention that $\mathcal{N}(\cdot;\cdot,\cdot)$ is linear with respect to the arguments to the right of the semi-colon. We suppose that u is the unique solution to the variational problem: find u in X such that

$$\mathcal{N}(u;u,v) = 0 \quad \forall v \in Y. \tag{1}$$

Problem (1) can be thought of as the weak formulation of a nonlinear partial differential equation on X whose unique solution is $u \in X$. In practice (1) cannot be solved in closed form but needs to be approximated numerically. For the purposes of this paper, we shall consider general *hp*-version finite element approximations to (1). In order to construct a Galerkin approximation to this problem, we consider a sequence of finite-dimensional spaces $\{X_{h,p}\}$, parameterised by the positive discretisation parameters h and p. Simultaneously, consider a sequence of finite-dimensional spaces $\{Y_{h,p}\}$. For the purposes of this paper, $X_{h,p}$ and $Y_{h,p}$ can be thought of as finite element spaces consisting of piecewise polynomial functions of degree p on a partition $\mathcal{T}_h$, of granularity h, of the computational domain. The (standard) Galerkin approximation $u_{h,p}$ of u is then sought in $X_{h,p}$ as the solution of the finite-dimensional problem

$$\mathcal{N}_{h,p}(u_{h,p};u_{h,p},v_{h,p}) = 0 \quad \forall v_{h,p} \in Y_{h,p}, \tag{2}$$

where $\mathcal{N}_{h,p}(\cdot;\cdot,\cdot) : X_{h,p} \times X_{h,p} \times Y_{h,p} \to \mathbb{R}$. The computation of $u_{h,p}$ defined in (2) involves the numerical solution of a potentially very large number of coupled nonlinear equations, which can be extremely computationally expensive. The key idea of the two-grid approach is as follows: given 'coarser' finite element spaces $X_{H,P} \subseteq X_{h,p}$ and $Y_{H,P} \subseteq Y_{h,p}$, first solve the nonlinear problem: find $u_{H,P} \in X_{H,P}$ such that

$$\mathcal{N}_{H,P}(u_{H,P};u_{H,P},v_{H,P}) = 0 \quad \forall v_{H,P} \in Y_{H,P}. \tag{3}$$

Finally, using $u_{H,P}$ as appropriate data, compute the two-grid approximation of (1) by solving the problem: find $u_{2G} \in X_{h,p}$ such that

$$\mathcal{N}_{h,p}(u_{H,P};u_{2G},v_{h,p}) = 0 \quad \forall v_{h,p} \in Y_{h,p}. \tag{4}$$

We emphasise that this latter problem is *linear*.

In this article we analyse the *hp*-version of the two-grid IP DGFEM, see [6], for the numerical solution of the following quasilinear elliptic boundary-value problem:

$$-\nabla \cdot (\mu(\boldsymbol{x}, |\nabla u|)\nabla u) = f \quad \text{in } \Omega, \tag{5}$$

$$u = 0 \quad \text{on } \Gamma, \tag{6}$$

where Ω is a bounded polygonal domain in $\mathbb{R}^2$, with boundary Γ and $f \in \mathrm{L}_2(\Omega)$. Here, we assume that the nonlinearity μ satisfies the following conditions:

(A1) $\mu \in \mathrm{C}^0(\bar{\Omega} \times [0, \infty))$ and

(A2) there exists positive constants m_μ and M_μ such that the following monotonicity property is satisfied:

$$m_\mu(t - s) \leq \mu(\boldsymbol{x}, t)t - \mu(\boldsymbol{x}, s)s \leq M_\mu(t - s), \quad t \geq s \geq 0, \boldsymbol{x} \in \bar{\Omega}. \tag{7}$$

From [18, Lemma 2.1] we note that, as μ satisfies (7), there exists constants C_1 and C_2, $C_1 \geq C_2 > 0$, such that for all vectors $\boldsymbol{v}, \boldsymbol{w} \in \mathbb{R}^2$ and all $\boldsymbol{x} \in \bar{\Omega}$,

$$|\mu(\boldsymbol{x}, |\boldsymbol{v}|)\boldsymbol{v} - \mu(\boldsymbol{x}, |\boldsymbol{w}|)\boldsymbol{w}| \leq C_1|\boldsymbol{v} - \boldsymbol{w}|, \tag{8}$$

$$C_2|\boldsymbol{v} - \boldsymbol{w}|^2 \leq (\mu(\boldsymbol{x}, |\boldsymbol{v}|)\boldsymbol{v} - \mu(\boldsymbol{x}, |\boldsymbol{w}|)\boldsymbol{w}) \cdot (\boldsymbol{v} - \boldsymbol{w}). \tag{9}$$

By setting $s = 0$ in (7) we deduce the following bound on μ:

$$m_\mu \leq \mu(\boldsymbol{x}, t) \leq M_\mu, \quad t \geq 0, \boldsymbol{x} \in \bar{\Omega}. \tag{10}$$

For ease of notation we shall suppress the dependence of μ on $\boldsymbol{x}$ and write $\mu(t)$ instead of $\mu(\boldsymbol{x}, t)$. We note that a number of physical models which arise in continuum mechanics, such as the Carreau law $\mu(t) = k_\infty + (k_0 - k_\infty)(1 + \lambda t^2)^{(\theta-2)/2}$, with $k_0 > k_\infty > 0$ and $\theta \in (1, 2]$, fulfil the above assumptions.

In contrast to the work undertaken in [6], where $\mu = \mu(u)$ (semilinear problem), in this article we consider the quasilinear case when the nonlinear diffusion term may depend on $|\nabla u|$. In addition, in the current paper the DGFEM will be analysed within the more general setting of *hp*-version methods. The analysis in [6] relies on a suitable duality argument in order to optimally bound the resulting L_2-terms; it is shown that for convergence, the coarse and fine mesh sizes H and h, respectively, should satisfy $H = \mathcal{O}(\sqrt{h})$, when the polynomial degree is (uniformly) set equal to one. The convergence analysis undertaken in this article for the two-grid IP DGFEM applied to (5)–(6) indicates that the mesh and polynomial distribution of both the fine and coarse finite element spaces should grow at roughly the same rate; numerical experiments demonstrating the optimality of these theoretical bounds are given in [10], cf. Remark 3.2 below. One of the key issues concerning the implementation of two-grid methods is the automatic construction of the fine and coarse finite element spaces. With this in mind, we derive a computable *a posteriori* error bound which includes both fine and coarse mesh error indicators; these are subsequently exploited within an *hp*-refinement algorithm which is capable of automatically designing the coarse and fine finite element spaces in an efficient manner.

The outline of the rest of this article is as follows. Section 2 introduces the two-grid *hp*-version of the IP DGFEM for the numerical approximation of (5)–(6). In Sect. 3 we derive both *a priori* and *a posteriori* bounds on the error, measured in terms of the corresponding (DGFEM) energy norm, for the proposed numerical scheme. Section 4 is devoted to the

design of an *hp*-adaptive algorithm which can construct the coarse and fine *hp*-finite element spaces in an automatic fashion. The performance of the proposed adaptive strategy is demonstrated in Sect. 5; we refer to [10] for numerical experiments which validate the sharpness of the *a priori* error bounds. Finally, in Sect. 6 we summarise the work presented in this paper and draw some conclusions.

2 Two-Grid *hp*-Version IP DGFEM

In this section we discuss the numerical approximation of the problem (5)–(6) based on employing both the *hp*-version of the (standard) IP DGFEM, together with its so-called two-grid variant. To this end, in the following section we first introduce the necessary notation.

2.1 Meshes, Spaces, and Trace Operators

We consider shape-regular meshes $\mathcal{T}_h$ that partition $\Omega \subset \mathbb{R}^2$ into open disjoint triangles and/or parallelograms κ, such that $\overline{\Omega} = \bigcup_{\kappa \in \mathcal{T}_h} \overline{\kappa}$. By h_κ we denote the element diameter of $\kappa \in \mathcal{T}_h$, $h = \max_{\kappa \in \mathcal{T}_h} h_\kappa$, and $\boldsymbol{n}_\kappa$ signifies the unit outward normal vector to κ. We allow the meshes $\mathcal{T}_h$ to be *1-irregular*, i.e., each edge of any one element $\kappa \in \mathcal{T}_h$ contains at most one hanging node (which, for simplicity, we assume to be the midpoint of the corresponding edge). Here, we suppose that $\mathcal{T}_h$ is *regularly reducible* (cf. [22, Sect. 7.1]), i.e., there exists a shape-regular conforming (regular) mesh $\mathcal{T}_{\widetilde{h}}$ (consisting of triangles and parallelograms) such that the closure of each element in $\mathcal{T}_h$ is a union of closures of elements of $\mathcal{T}_{\widetilde{h}}$, and that there exists a constant $C > 0$, independent of the element sizes, such that for any two elements $\kappa \in \mathcal{T}_h$ and $\widetilde{\kappa} \in \mathcal{T}_{\widetilde{h}}$ with $\widetilde{\kappa} \subseteq \kappa$ we have $h_\kappa / \widetilde{h}_{\widetilde{\kappa}} \leq C$. Note that these assumptions imply that the family $\{\mathcal{T}_h\}_{h>0}$ is of *bounded local variation*, i.e., there exists a constant $\rho_1 \geq 1$, independent of the element sizes, such that

$$\rho_1^{-1} \leq h_\kappa / h_{\kappa'} \leq \rho_1, \tag{11}$$

for any pair of elements $\kappa, \kappa' \in \mathcal{T}_h$ which share a common edge $e = \partial\kappa \cap \partial\kappa'$.

To each $\kappa \in \mathcal{T}_h$ we assign a polynomial degree $p_\kappa \geq 1$ (local approximation order) and define the degree vector $\boldsymbol{p} = \{p_\kappa : \kappa \in \mathcal{T}_h\}$. We suppose that $\boldsymbol{p}$ is also of bounded local variation, i.e., there exists a constant $\rho_2 \geq 1$, independent of the element sizes and $\boldsymbol{p}$, such that, for any pair of neighbouring elements $\kappa, \kappa' \in \mathcal{T}_h$,

$$\rho_2^{-1} \leq p_\kappa / p_{\kappa'} \leq \rho_2. \tag{12}$$

With this notation, we introduce the finite element space

$$V(\mathcal{T}_h, \boldsymbol{p}) = \{v \in \mathrm{L}_2(\Omega) : v|_\kappa \in \mathcal{S}_{p_\kappa}(\kappa)\ \forall \kappa \in \mathcal{T}_h\},$$

where

$$\mathcal{S}_{p_\kappa}(\kappa) = \begin{cases} \mathcal{P}_{p_\kappa}(\kappa) & \text{if } \kappa \text{ is a triangle,} \\ \mathcal{Q}_{p_\kappa}(\kappa) & \text{if } \kappa \text{ is a parallelogram.} \end{cases}$$

Here, given $p \geq 0$, $\mathcal{P}_p(\kappa)$ denotes the space of polynomials of degree at most p on κ, while $\mathcal{Q}_p(\kappa)$ is the space of polynomials of degree at most p in each variable on κ.

We shall now define some suitable edge operators that are required for the definition of the IP DGFEM. To this end, associated with the mesh $\mathcal{T}_h$, we denote by $\mathcal{E}_h^{\mathcal{I}}$ the set of all interior edges of the partition $\mathcal{T}_h$ of Ω, and by $\mathcal{E}_h^{\mathcal{B}}$ the set of all boundary edges of $\mathcal{T}_h$. In addition, $\mathcal{E}_h = \mathcal{E}_h^{\mathcal{B}} \cup \mathcal{E}_h^{\mathcal{I}}$ denotes the set of all edges in the mesh $\mathcal{T}_h$.

Let v and $\boldsymbol{q}$ be scalar- and vector-valued functions, respectively, which are smooth inside each element $\kappa \in \mathcal{T}_h$. Given two adjacent elements, $\kappa^+, \kappa^- \in \mathcal{T}_h$ which share a common edge $e \in \mathcal{E}_h^{\mathcal{I}}$, i.e., $e = \partial\kappa^+ \cap \partial\kappa^-$, we write $v^\pm$ and $\boldsymbol{q}^\pm$ to denote the traces of the functions v and $\boldsymbol{q}$, respectively, on the edge e, taken from the interior of $\kappa^\pm$, respectively. With this notation, the averages of v and $\boldsymbol{q}$ at $\boldsymbol{x} \in e$ are given by

$$\{\!\{v\}\!\} = \frac{1}{2}(v^+ + v^-), \qquad \{\!\{\boldsymbol{q}\}\!\} = \frac{1}{2}(\boldsymbol{q}^+ + \boldsymbol{q}^-),$$

respectively. Similarly, the jumps of v and $\boldsymbol{q}$ at $\boldsymbol{x} \in e$ are given by

$$[\![v]\!] = v^+\boldsymbol{n}_{\kappa^+} + v^-\boldsymbol{n}_{\kappa^-}, \qquad [\![\boldsymbol{q}]\!] = \boldsymbol{q}^+ \cdot \boldsymbol{n}_{\kappa^+} + \boldsymbol{q}^- \cdot \boldsymbol{n}_{\kappa^-},$$

respectively, where $\boldsymbol{n}_{\kappa^\pm}$ denotes the unit outward normal vector on $\partial\kappa^\pm$, respectively. On a boundary edge $e \in \mathcal{E}_h^{\mathcal{B}}$, we set $\{\!\{v\}\!\} = v$, $\{\!\{\boldsymbol{q}\}\!\} = \boldsymbol{q}$, $[\![v]\!] = v\boldsymbol{n}$ and $[\![\boldsymbol{q}]\!] = \boldsymbol{q} \cdot \boldsymbol{n}$, with $\boldsymbol{n}$ denoting the unit outward normal vector on the boundary Γ.

For an edge $e \in \mathcal{E}_h$, we define h_e to be the length of the edge; moreover, the edge polynomial degree p_e is defined by

$$p_e = \begin{cases} \max(p_\kappa, p_{\kappa'}), & \text{if } e = \partial\kappa \cap \partial\kappa' \in \mathcal{E}_h^{\mathcal{I}}, \\ p_\kappa, & \text{if } e = \partial\kappa \cap \Gamma \in \mathcal{E}_h^{\mathcal{B}}. \end{cases} \tag{13}$$

Finally, we recall the following inverse trace inequalities.

Lemma 2.1 *We note that, for an edge e of an element $\kappa \in \mathcal{T}_h$, the following* inverse trace inequalities *hold: there exists a positive constant C_{trace}, independent of h and $\boldsymbol{p}$, such that*

$$\|w\|^2_{\mathrm{L}_2(e)} \le C_{\text{trace}} \frac{p_\kappa^2}{h_e} \|w\|^2_{\mathrm{L}_2(\kappa)} \quad \textit{and} \quad \|\nabla w\|^2_{\mathrm{L}_2(e)} \le C_{\text{trace}} \frac{p_\kappa^2}{h_e} \|\nabla w\|^2_{\mathrm{L}_2(\kappa)}$$

for all $w \in V(\mathcal{T}_h, \boldsymbol{p})$.

Proof See [24, Theorem 4.76] for details. □

2.2 Interior Penalty DGFEM Discretisation

In this section we first introduce the so-called *standard* IP DGFEM for the numerical approximation of the problem (5)–(6). To this end, given a (fine) mesh $\mathcal{T}_h$ partition of Ω, together with a corresponding polynomial degree vector $\boldsymbol{p}$, the standard IP DGFEM is defined as follows: find $u_{h,p} \in V(\mathcal{T}_h, \boldsymbol{p})$ such that

$$A_{h,p}(u_{h,p}; u_{h,p}, v_{h,p}) = F_{h,p}(v_{h,p}) \tag{14}$$

for all $v_{h,p} \in V(\mathcal{T}_h, \boldsymbol{p})$, where

$$A_{h,p}(\psi;u,v)=\sum_{\kappa\in\mathcal{T}_h}\int_\kappa \mu(|\nabla\psi|)\nabla u\cdot\nabla v\,\mathrm{d}\boldsymbol{x}+\sum_{e\in\mathcal{E}_h}\int_e \sigma_{h,p}[\![u]\!]\cdot[\![v]\!]\,\mathrm{d}s$$
$$-\sum_{e\in\mathcal{E}_h}\int_e \{\!\{\mu(|\nabla_h\psi|)\nabla_h u\}\!\}\cdot[\![v]\!]\,\mathrm{d}s+\theta\sum_{e\in\mathcal{E}_h}\int_e \{\!\{\mu(h_e^{-1}|[\![\psi]\!]|)\nabla_h v\}\!\}\cdot[\![u]\!]\,\mathrm{d}s,$$
$$F_{h,p}(v)=\sum_{\kappa\in\mathcal{T}_h}\int_\kappa f v\,\mathrm{d}\boldsymbol{x},$$

and ∇_h is used to denote the broken gradient operator, defined elementwise. Here, $\theta\in[-1,1]$ and the *interior penalty parameter* $\sigma_{h,p}$ is defined as follows:

$$\sigma_{h,p}=\gamma\frac{p_e^2}{h_e},$$

where $\gamma>0$ is a constant. We note that, due to the condition on the nonlinearity (7), the interior penalty stabilisation may be selected independent of $\mu(\cdot)$, provided the penalty parameter is chosen sufficiently large (independent of local element sizes and polynomial degrees) such that it is greater than a constant $\gamma_{\min}$, dependent on m_μ and M_μ, cf. Lemma 2.2 and Remark 2.3 below; see, also, [12, 13], for example.

Remark 2.1 The IP DGFEM defined in (14) is identical to the parameterised DGFEMs considered in [13].

Remark 2.2 In the case of an inhomogeneous boundary condition $u=g$ on Γ, the right-hand side linear functional $F_{h,p}(\cdot)$ must be replaced by

$$F_{h,p}(v)=\sum_{\kappa\in\mathcal{T}_h}\int_\kappa f v\,\mathrm{d}\boldsymbol{x}+\sum_{e\in\mathcal{E}_h^{\mathcal{B}}}\int_e \sigma_{h,p}g v\,\mathrm{d}s,$$

and the fourth term in the nonlinear form $A_{h,p}$ is replaced by

$$\theta\sum_{e\in\mathcal{E}_h^{\mathcal{I}}}\int_e \{\!\{\mu(h_e^{-1}|[\![\psi]\!]|)\nabla_h v\}\!\}\cdot[\![u]\!]\,\mathrm{d}s+\theta\sum_{e\in\mathcal{E}_h^{\mathcal{B}}}\int_e \mu(h_e^{-1}|[\![\psi]\!]|)\nabla_h v\cdot\boldsymbol{n}(u-g)\,\mathrm{d}s,$$

cf. [13]

Introducing the *energy norm*

$$\|v\|_{h,p}^2=\|\nabla_h v\|_{\mathrm{L}_2(\Omega)}^2+\sum_{e\in\mathcal{E}_h}\int_e \sigma_{h,p}|[\![v]\!]|^2\,\mathrm{d}s,$$

on the class of spaces $H^1(\Omega)+V(\mathcal{T}_h,\boldsymbol{p})$, the general form of the nonlinear form $A_{h,p}(\psi;\cdot,\cdot)$ is coercive, in the sense that the following lemma holds for sufficiently large γ.

Lemma 2.2 *There exists a positive constant $\gamma_{\min}$, such that for any $\gamma\geq\gamma_{\min}$, there exists a coercivity constant $C_c=C_c(m_\mu,M_\mu,C_{\mathrm{trace}},\rho_1,\rho_2)>0$, independent of h and $\boldsymbol{p}$, such that*

$$A_{h,p}(\psi;v,v)\geq C_c\,\|v\|_{h,p}^2 \tag{15}$$

for all $\psi,v\in V(\mathcal{T}_h,\boldsymbol{p})$.

Proof By application of (10), Lemma 2.1 and the arithmetic-geometric mean inequality, $2ab \leq \varepsilon a^2 + \varepsilon^{-1} b^2$ with $\varepsilon = \delta \sigma_{h,p}^{-1}$ and $\delta > 1$, we have that

$$
\begin{aligned}
A_{h,p}(\psi; v, v) &= \sum_{\kappa \in \mathcal{T}_h} \int_\kappa \mu(|\nabla \psi|) |\nabla v|^2 \, \mathrm{d}\boldsymbol{x} + \sum_{e \in \mathcal{E}_h} \int_e \sigma_{h,p} |[\![v]\!]|^2 \, \mathrm{d}s \\
&\quad - \sum_{e \in \mathcal{E}_h} \int_e \{\!\{ \mu(|\nabla \psi|) \nabla v \}\!\} \cdot [\![v]\!] \, \mathrm{d}s + \theta \sum_{e \in \mathcal{E}_h} \int_e \{\!\{ \mu(h_e^{-1} |[\![\psi]\!]|) \nabla v \}\!\} [\![v]\!] \, \mathrm{d}s \\
&\geq \sum_{\kappa \in \mathcal{T}_h} \int_\kappa \mu(|\nabla \psi|) |\nabla v|^2 \, \mathrm{d}\boldsymbol{x} + \sum_{e \in \mathcal{E}_h} \int_e \sigma_{h,p} |[\![v]\!]|^2 \, \mathrm{d}s \\
&\quad - \sum_{e \in \mathcal{E}_h} \int_e \frac{\varepsilon}{2} \left(|\{\!\{ \mu(|\nabla \psi|) \nabla v \}\!\}|^2 + \theta^2 |\{\!\{ \mu(h_e^{-1} |[\![\psi]\!]|) \nabla v \}\!\}|^2 \right) \mathrm{d}s \\
&\quad - \sum_{e \in \mathcal{E}_h} \int_e \varepsilon^{-1} |[\![v]\!]|^2 \, \mathrm{d}s \\
&\geq m_\mu \sum_{\kappa \in \mathcal{T}_h} \|\nabla v\|^2_{\mathrm{L}_2(\kappa)} + (1 - \delta^{-1}) \gamma \sum_{e \in \mathcal{E}_h} \int_e p_e^2 h_e^{-1} |[\![v]\!]|^2 \, \mathrm{d}s \\
&\quad - M_\mu^2 C_\rho \delta \gamma^{-1} \sum_{\kappa \in \mathcal{T}_h} p_\kappa^{-2} h_e \, \|\nabla v\|^2_{\mathrm{L}_2(\partial \kappa)} \\
&\geq \min(m_\mu - C_{\mathrm{trace}} M_\mu^2 C_\rho \delta \gamma^{-1}, (1 - \delta^{-1}) \gamma) \, \|v\|^2_{h,p} \,,
\end{aligned}
$$

where C_ρ is a positive constant dependent on ρ_1 and ρ_2 from (11) and (12), respectively. Thereby, the statement of the lemma immediately follows, provided $\gamma > C_{\mathrm{trace}} M_\mu^2 C_\rho \delta m_\mu^{-1}$, with δ sufficiently large. □

Remark 2.3 From the proof of Lemma 2.2, we observe that the requirement on the parameter γ appearing in the definition of the interior penalty parameter $\sigma_{h,p}$ is that $\gamma > C_{\mathrm{trace}} M_\mu^2 C_\rho \delta m_\mu^{-1}$, where C_ρ is a positive constant dependent on ρ_1 and ρ_2 from (11) and (12), respectively. Thereby, a reduction in the magnitude of the constant m_μ appearing in the lower bound (7) leads to a corresponding increase in the minimal value of γ needed to guarantee coercivity.

2.3 Two-Grid Interior Penalty Discretisation

In this section, we now proceed to introduce the so-called two-grid IP DGFEM approximation to (5)–(6). To this end, we consider two partitions $\mathcal{T}_h$ and $\mathcal{T}_H$ of the computational domain Ω, of granularity h and H, respectively. Here, we refer to $\mathcal{T}_h$ and $\mathcal{T}_H$ as the fine and coarse mesh partitions of Ω, respectively. In particular, we assume that $\mathcal{T}_h$ and $\mathcal{T}_H$ are nested in the sense that, for any $\kappa_h \in \mathcal{T}_h$ there exists an element $\kappa_H \in \mathcal{T}_H$ such that $\bar{\kappa}_h \subseteq \bar{\kappa}_H$. Moreover, to each mesh $\mathcal{T}_h$ and $\mathcal{T}_H$, we associate a corresponding polynomial degree distribution $\boldsymbol{p} = \{p_\kappa : \kappa \in \mathcal{T}_h\}$ and $\boldsymbol{P} = \{P_\kappa : \kappa \in \mathcal{T}_H\}$, respectively, with the property that, given $\kappa_h \in \mathcal{T}_h$ and the associated $\kappa_H \in \mathcal{T}_H$, such that $\bar{\kappa}_h \subseteq \bar{\kappa}_H$, the corresponding polynomial degrees satisfy the following condition:

$$
p_{\kappa_h} \geq P_{\kappa_H} .
$$

Given $\mathcal{T}_h$, $\boldsymbol{p}$ and $\mathcal{T}_H$, $\boldsymbol{P}$, we may construct the corresponding fine and coarse *hp*-finite element spaces $V(\mathcal{T}_h, \boldsymbol{p})$ and $V(\mathcal{T}_H, \boldsymbol{P})$, respectively, which satisfy the following condition: $V(\mathcal{T}_H, \boldsymbol{P}) \subseteq V(\mathcal{T}_h, \boldsymbol{p})$.

With this notation, we now introduce the *hp*-version of the two-grid algorithm [6, Algorithm 1] for the IP DGFEM discretisation of (5)–(6):

1. (Nonlinear solve) Compute the coarse grid approximation $u_{H,P} \in V(\mathcal{T}_H, \boldsymbol{P})$ such that

$$A_{H,P}(u_{H,P}; u_{H,P}, v_{H,P}) = F_{H,P}(v_{H,P}) \tag{16}$$

   for all $v_{H,P} \in V(\mathcal{T}_H, \boldsymbol{P})$.
2. (Linear solve) Determine the fine grid solution $u_{2G} \in V(\mathcal{T}_h, \boldsymbol{p})$ such that

$$A_{h,p}(u_{H,P}; u_{2G}, v_{h,p}) = F_{h,p}(v_{h,p}) \tag{17}$$

   for all $v_{h,p} \in V(\mathcal{T}_h, \boldsymbol{p})$.

Existence and uniqueness of the solution $u_{H,P}$ for this formulation is demonstrated in [12]. The formulation (17) is a interior penalty discretisation of a linear elliptic PDE, where the coefficient $\mu(|\nabla_h u_{H,P}|)$ is a known function; thereby, the existence and uniqueness of the solution u_{2G} to this problem follows immediately, cf., for example, [25, 28].

3 Error Analysis

In this section, we develop the *a priori* and *a posteriori* error analysis of the two-grid IP DGFEM defined by (16)–(17).

3.1 *A Priori* Error Bound

We first recall the following *a priori* error bound for the standard IP DGFEM approximation (14) of the quasilinear problem (5)–(6).

Lemma 3.1 *Assuming that* $u \in \mathrm{C}^1(\Omega)$ *and* $u|_\kappa \in \mathrm{H}^{k_\kappa}(\kappa)$, $k_\kappa \geq 2$, *for* $\kappa \in \mathcal{T}_h$ *then the solution* $u_{h,p} \in V(\mathcal{T}_h, \boldsymbol{p})$ *of* (14) *satisfies the error bound*

$$\left\|u - u_{h,p}\right\|_{h,p}^2 \leq C_3 \sum_{\kappa \in \mathcal{T}_h} \frac{h_\kappa^{2s_\kappa - 2}}{p_\kappa^{2k_\kappa - 3}} \|u\|_{H^{k_\kappa}(\kappa)}^2 \tag{18}$$

with $1 \leq s_k \leq \min\{p_\kappa + 1, k_\kappa\}$, $p_\kappa \geq 1$, *for* $\kappa \in \mathcal{T}_h$, *and* C_3 *is a positive constant independent of* u, h *and* $\boldsymbol{p}$, *but depends on constants* m_μ, M_μ, C_1 *and* C_2 *from the monotonicity properties of* $\mu(\cdot)$.

Proof See [13]. □

Remark 3.1 We note that this error bound also clearly holds for the two-grid coarse solution $u_{H,P}$ defined in (16) with the energy norm $\|\cdot\|_{h,p}$ replaced by $\|\cdot\|_{H,P}$, and similarly the mesh size and polynomial degrees h_κ and p_κ replaced by H_κ and P_κ, respectively.

Employing Lemma 3.1, we now deduce the following error bound for the two-grid approximation defined in (16)–(17).

Theorem 3.1 *Assuming that* $u \in \mathrm{C}^1(\Omega)$, $u|_\kappa \in \mathrm{H}^{k_\kappa}(\kappa)$, $k_\kappa \geq 2$, *for* $\kappa \in \mathcal{T}_h$ *and* $u|_\kappa \in \mathrm{H}^{K_\kappa}(\kappa)$, $K_\kappa \geq 2$, *for* $\kappa \in \mathcal{T}_H$, *then the solution* $u_{2G} \in V(\mathcal{T}_h, \boldsymbol{p})$ *of* (17) *satisfies the error bounds*

$$\left\|u_{h,p} - u_{2G}\right\|_{h,p}^2 \leq C_4 \sum_{\kappa \in \mathcal{T}_H} \frac{H_\kappa^{2S_\kappa - 2}}{P_\kappa^{2K_\kappa - 3}} \|u\|_{H^{K_\kappa}(\kappa)}^2, \tag{19}$$

$$\|u - u_{2G}\|_{h,p}^2 \leq C_3 \sum_{\kappa \in \mathcal{T}_h} \frac{h_\kappa^{2s_\kappa - 2}}{p_\kappa^{2k_\kappa - 3}} \|u\|_{H^{k_\kappa}(\kappa)}^2 + C_4 \sum_{\kappa \in \mathcal{T}_H} \frac{H_\kappa^{2S_\kappa - 2}}{P_\kappa^{2K_\kappa - 3}} \|u\|_{H^{K_\kappa}(\kappa)}^2, \tag{20}$$

with $1 \leq s_k \leq \min\{p_\kappa + 1, k_\kappa\}$, $p_\kappa \geq 1$, *for* $\kappa \in \mathcal{T}_h$, $1 \leq S_k \leq \min\{P_\kappa + 1, K_\kappa\}$, $P_\kappa \geq 1$, *for* $\kappa \in \mathcal{T}_H$, *and* C_3 *and* C_4 *are positive constants independent of* u, h, H, $\boldsymbol{p}$ *and* $\boldsymbol{P}$, *but depends on constants* m_μ, M_μ, C_1 *and* C_2 *from the monotonicity properties of* $\mu(\cdot)$.

Proof By application of the triangle inequality, we get

$$\|u - u_{2G}\|_{h,p} \leq \left\|u - u_{h,p}\right\|_{h,p} + \left\|u_{2G} - u_{h,p}\right\|_{h,p}. \tag{21}$$

We note that the first term on the right-hand side of (21) may be bounded by employing Lemma 3.1. Let us now deal with the second term; to this end, from (14) and (17) we have that

$$A_{h,p}(u_{H,P}; u_{2G}, v_{h,p}) = A_{h,p}(u_{h,p}; u_{h,p}, v_{h,p})$$

for all $v_{h,p}$ in $V(\mathcal{T}_h, \boldsymbol{p})$. Let $\phi = u_{2G} - u_{h,p} \in V(\mathcal{T}_h, \boldsymbol{p})$; then from Lemma 2.2, we get

$$\begin{aligned} C_c \left\|u_{2G} - u_{h,p}\right\|_{h,p}^2 &\leq A_{h,p}(u_{H,P}; u_{2G} - u_{h,p}, \phi) \\ &= A_{h,p}(u_{H,P}; u_{2G}, \phi) - A_{h,p}(u_{H,P}; u_{h,p}, \phi) \\ &= A_{h,p}(u_{h,p}; u_{h,p}, \phi) - A_{h,p}(u_{H,P}; u_{h,p}, \phi) \\ &\equiv T_1 + T_2 + T_3, \end{aligned} \tag{22}$$

where

$$T_1 = \sum_{\kappa \in \mathcal{T}_h} \int_\kappa (\mu(|\nabla u_{h,p}|) - \mu(|\nabla u_{H,P}|)) \nabla u_{h,p} \cdot \nabla \phi \, \mathrm{d}\boldsymbol{x},$$

$$T_2 = -\sum_{e \in \mathcal{E}_h} \int_e \{\!\{(\mu(|\nabla u_{h,p}|) - \mu(|\nabla u_{H,P}|)) \nabla u_{h,p}\}\!\} \cdot [\![\phi]\!] \, \mathrm{d}s,$$

$$T_3 = \theta \sum_{e \in \mathcal{E}_h} \int_e \{\!\{(\mu(h_e^{-1}|[\![u_{h,p}]\!]|) - \mu(h_e^{-1}|[\![u_{H,P}]\!]|)) \nabla \phi\}\!\} \cdot [\![u_{h,p}]\!] \, \mathrm{d}s.$$

To bound term T_1, we employ the triangle inequality, (8), (10) and Lemma 3.1; thereby, we deduce that

$$\begin{aligned} |T_1| \leq &\sum_{\kappa \in \mathcal{T}_h} \int_\kappa |\mu(|\nabla u_{h,p}|) \nabla u_{h,p} - \mu(|\nabla u_{H,P}|) \nabla u_{H,P}| \cdot |\nabla \phi| \, \mathrm{d}\boldsymbol{x} \\ &+ \sum_{\kappa \in \mathcal{T}_h} \int_\kappa |\mu(|\nabla u_{H,P}|) \nabla \left(u_{H,P} - u_{h,p}\right)| \cdot |\nabla \phi| \, \mathrm{d}\boldsymbol{x} \end{aligned}$$

$$
\begin{aligned}
&\leq \left(C_1 + M_\mu\right) \sum_{\kappa\in\mathcal{T}_h} \int_\kappa \left|\nabla\left(u_{h,p} - u_{H,P}\right)\right| \cdot |\nabla\phi| \,\mathrm{d}\boldsymbol{x} \\
&\leq \left(C_1 + M_\mu\right) \left\{ \left(\sum_{\kappa\in\mathcal{T}_h} \left\|\nabla(u - u_{h,p})\right\|^2_{\mathrm{L}_2(\kappa)} \right)^{\frac{1}{2}} + \left(\sum_{\kappa\in\mathcal{T}_H} \left\|\nabla(u - u_{H,P})\right\|^2_{\mathrm{L}_2(\kappa)} \right)^{\frac{1}{2}} \right\} \|\nabla\phi\|_{\mathrm{L}_2(\kappa)} \\
&\leq \left(C_1 + M_\mu\right) C_3 \left\{ \left(\sum_{\kappa\in\mathcal{T}_h} \frac{h_\kappa^{2s_k-2}}{p_\kappa^{2k_\kappa-3}} \|u\|^2_{\mathrm{H}^{k_\kappa}(\kappa)} \right)^{\frac{1}{2}} + \left(\sum_{\kappa\in\mathcal{T}_H} \frac{H_\kappa^{2S_k-2}}{P_\kappa^{2K_\kappa-3}} \|u\|^2_{\mathrm{H}^{K_\kappa}(\kappa)} \right)^{\frac{1}{2}} \right\} \|\phi\|_{h,p} .
\end{aligned} \tag{23}
$$

Proceeding in an analogous manner for term T_2, we get that

$$
\begin{aligned}
|T_2| &\leq \sum_{e\in\mathcal{E}_h} \int_e \left\{\!\!\left\{ |\mu(|\nabla u_{h,p}|)\nabla u_{h,p} - \mu(|\nabla u_{H,P}|)\nabla u_{H,P}| \right\}\!\!\right\} \cdot |[\![\phi]\!]| \,\mathrm{d}s \\
&\quad + \sum_{e\in\mathcal{E}_h} \int_e \left\{\!\!\left\{ |\mu(|\nabla u_{H,P}|)\nabla\left(u_{H,P} - u_{h,p}\right)| \right\}\!\!\right\} \cdot |[\![\phi]\!]| \,\mathrm{d}s \\
&\leq \left(C_1 + M_\mu\right) \sum_{e\in\mathcal{E}_h} \int_e \left\{\!\!\left\{ |\nabla\left(u_{h,p} - u_{H,P}\right)| \right\}\!\!\right\} \cdot |[\![\phi]\!]| \,\mathrm{d}s \\
&\leq \left(C_1 + M_\mu\right) \left(\sum_{e\in\mathcal{E}_h} \int_e \sigma_{h,p} |[\![\phi]\!]|^2 \,\mathrm{d}s \right)^{\frac{1}{2}} \\
&\quad \times \left\{ \left(\sum_{e\in\mathcal{E}_h} \sigma_{h,p}^{-1} \left\|\left\{\!\!\left\{ |\nabla(u - u_{h,p})| \right\}\!\!\right\}\right\|^2_{\mathrm{L}_2(e)} \right)^{\frac{1}{2}} + \left(\sum_{e\in\mathcal{E}_h} \sigma_{h,p}^{-1} \left\|\left\{\!\!\left\{ |\nabla(u - u_{H,P})| \right\}\!\!\right\}\right\|^2_{\mathrm{L}_2(e)} \right)^{\frac{1}{2}} \right\} .
\end{aligned}
$$

Applying Lemma 2.1, inequalities (11) and (12), and Lemma 3.1 gives

$$
\begin{aligned}
|T_2| &\leq \left(C_1 + M_\mu\right) C_\rho C_{\mathrm{trace}} \gamma^{-\frac{1}{2}} \|\phi\|_{h,p} \\
&\quad \times \left\{ \left(\sum_{\kappa\in\mathcal{T}_h} \left\|\nabla(u - u_{h,p})\right\|^2_{\mathrm{L}_2(\kappa)} \right)^{\frac{1}{2}} + \left(\sum_{\kappa\in\mathcal{T}_h} \left\|\nabla(u - u_{H,P})\right\|^2_{\mathrm{L}_2(\kappa)} \right)^{\frac{1}{2}} \right\} \\
&\leq \left(C_1 + M_\mu\right) C_3 C_\rho C_{\mathrm{trace}} \gamma^{-\frac{1}{2}} \|\phi\|_{h,p} \\
&\quad \times \left\{ \left(\sum_{\kappa\in\mathcal{T}_h} \frac{h_\kappa^{2s_k-2}}{p_\kappa^{2k_\kappa-3}} \|u\|^2_{\mathrm{H}^{k_\kappa}(\kappa)} \right)^{\frac{1}{2}} + \left(\sum_{\kappa\in\mathcal{T}_H} \frac{H_\kappa^{2S_k-2}}{P_\kappa^{2K_\kappa-3}} \|u\|^2_{\mathrm{H}^{K_\kappa}(\kappa)} \right)^{\frac{1}{2}} \right\} ,
\end{aligned} \tag{24}
$$

where the constant C_ρ depends on ρ_1 and ρ_2, from (11) and (12) respectively. We now consider the term T_3:

$$
\begin{aligned}
|T_3| &\leq \sum_{e\in\mathcal{E}_h} \int_e \left\{\!\!\left\{ |(\mu(h_e^{-1}|[\![u_{h,p}]\!]|) - \mu(h_e^{-1}|[\![u_{H,P}]\!]|))\nabla\phi| \right\}\!\!\right\} \cdot |[\![u_{h,p}]\!]| \,\mathrm{d}s \\
&\leq \sum_{e\in\mathcal{E}_h} \left\| \mu(h_e^{-1}|[\![u_{h,p}]\!]|) - \mu(h_e^{-1}|[\![u_{H,P}]\!]|) \right\|_{\mathrm{L}_\infty(e)} \left\|\left\{\!\!\left\{ |\nabla\phi| \right\}\!\!\right\}\right\|_{\mathrm{L}_2(e)} \left\|[\![u_{h,p}]\!]\right\|_{\mathrm{L}_2(e)} .
\end{aligned}
$$

We note that from inequality (10), we have

$$\begin{aligned}&\left\|\mu(h_e^{-1}|[\![u_{h,p}]\!]|)-\mu(h_e^{-1}|[\![u_{H,P}]\!]|)\right\|_{\mathrm{L}_\infty(e)}\\&\quad\le\left\|\mu(h_e^{-1}|[\![u_{h,p}]\!]|)\right\|_{\mathrm{L}_\infty(e)}+\left\|\mu(h_e^{-1}|[\![u_{H,P}]\!]|)\right\|_{\mathrm{L}_\infty(e)}\\&\quad\le 2M_\mu.\end{aligned}$$

Since $u\in\mathrm{H}_0^1(\Omega)$, we note that $|[\![u-u_{h,p}]\!]|=|[\![u_{h,p}]\!]|$; thereby,

$$|T_3|\le 2M_\mu\left(\sum_{e\in\mathcal{E}_h}\sigma_{h,p}^{-1}\left\|\{\!\{\nabla\phi\}\!\}\right\|_{\mathrm{L}_2(e)}^2\right)^{\frac{1}{2}}\left(\sum_{e\in\mathcal{E}_h}\int_e\sigma_{h,p}|[\![u-u_{h,p}]\!]|^2\,\mathrm{d}s\right)^{\frac{1}{2}}.$$

Applying Lemma 2.1, (11), (12) and Lemma 3.1 completes the bound for this term:

$$\begin{aligned}|T_3|&\le 2M_\mu C_\rho C_{\mathrm{trace}}\gamma^{-\frac{1}{2}}\left(\sum_{\kappa\in\mathcal{T}_h}\|\nabla\phi\|_{\mathrm{L}_2(\kappa)}^2\right)^{\frac{1}{2}}\left\|u-u_{h,p}\right\|_{h,p}\\&\le 2M_\mu C_3C_\rho C_{\mathrm{trace}}\gamma^{-\frac{1}{2}}\left(\sum_{\kappa\in\mathcal{T}_h}\frac{h_\kappa^{2s_k-2}}{p_\kappa^{2k_\kappa-3}}\|u\|_{\mathrm{H}^{k_\kappa}(\kappa)}^2\right)^{\frac{1}{2}}\|\phi\|_{h,p}.\end{aligned}\tag{25}$$

Inserting (23)–(25) into (22) and dividing both sides by $\|\phi\|_{h,p}$ gives

$$\left\|u_{2G}-u_{h,p}\right\|_{h,p}\le C\left\{\left(\sum_{\kappa\in\mathcal{T}_h}\frac{h_\kappa^{2s_k-2}}{p_\kappa^{2k_\kappa-3}}\|u\|_{\mathrm{H}^{k_\kappa}(\kappa)}^2\right)^{\frac{1}{2}}+\left(\sum_{\kappa\in\mathcal{T}_H}\frac{H_\kappa^{2S_k-2}}{P_\kappa^{2K_\kappa-3}}\|u\|_{\mathrm{H}^{K_\kappa}(\kappa)}^2\right)^{\frac{1}{2}}\right\}.$$

Noting that $V(\mathcal{T}_H,\boldsymbol{P})\subseteq V(\mathcal{T}_h,\boldsymbol{p})$, we deduce that

$$\left\|u_{2G}-u_{h,p}\right\|_{h,p}\le C_4\left(\sum_{\kappa\in\mathcal{T}_H}\frac{H_\kappa^{2S_k-2}}{P_\kappa^{2K_\kappa-3}}\|u\|_{\mathrm{H}^{K_\kappa}(\kappa)}^2\right)^{\frac{1}{2}},$$

which gives (19). Exploiting this inequality to bound the second term on the right-hand side of (21) and applying Lemma 3.1 to bound the first term, we deduce (20). □

Remark 3.2 We note that due to the dependence of the nonlinear coefficient μ on $|\nabla u|$, the error bound derived in Theorem 3.1 indicates that the mesh and polynomial distribution of both the fine and coarse finite element spaces $V(\mathcal{T}_h,\boldsymbol{p})$ and $V(\mathcal{T}_H,\boldsymbol{P})$, respectively, should grow at roughly the same rate, albeit the constants C_3 and C_4 present in the error bound being of differing sizes. Numerical experiments demonstrating the optimality of these theoretical bounds are given in [10]. We stress that this theoretical result by no means requires that $V(\mathcal{T}_h,\boldsymbol{p})$ and $V(\mathcal{T}_H,\boldsymbol{P})$ should be of the same dimension, but simply that the mesh-size and polynomial degree distributions should be enriched at roughly the same rate. This is analogous to the corresponding results for Schwarz-type preconditioners: to ensure scalability of the preconditioner, in the sense that the number of iterations required to achieve convergence is uniform, the coarse and fine meshes (in the case of an h-version method) must be refined at roughly the same rate, cf. [2], for example. As noted in the Introduction,

one of the key objectives of this article is to develop adaptive algorithms which are capable of automatically generating $V(\mathcal{T}_h, \boldsymbol{p})$ and $V(\mathcal{T}_H, \boldsymbol{P})$; this topic will be considered in the forthcoming sections. In particular, by exploiting the adaptive algorithm proposed in Sect. 4, in Sect. 5 we shall observe that there is indeed quite an off-set between the dimension of the fine and coarse finite element spaces.

Remark 3.3 As noted in Remark 3.2, Theorem 3.1 indicates that the mesh and polynomial distribution of both the fine and coarse finite element spaces $V(\mathcal{T}_h, \boldsymbol{p})$ and $V(\mathcal{T}_H, \boldsymbol{P})$, respectively, should grow at roughly the same rate. This is in contrast to the h-version *a priori* error analysis undertaken in [6] in the case when $\mu = \mu(u)$. Indeed, in that setting, by using a suitable duality argument (e.g., in convex domains) in order to optimally bound the resulting L_2-terms, it is shown that for convergence, the coarse and fine mesh sizes H and h, respectively, should satisfy $H = \mathcal{O}(\sqrt{h})$, when the polynomial degree is (uniformly) set equal to one. We point out that an alternative two-grid IP DGFEM to the one proposed in this article, cf. (16)–(17), may be developed, based on employing an incomplete Newton iteration on the fine finite element space $V(\mathcal{T}_h, \boldsymbol{p})$. More precisely, we define the nonlinear form

$$(u, v) \mapsto N_{h,p}(u, v) := A_{h,p}(u; u, v), \quad u, v \in V(\mathcal{T}_h, \boldsymbol{p})$$

and write $N'_{h,p}[u](\phi, v)$ to denote the Fréchet derivative of $u \mapsto N_{h,p}(u, v)$, for fixed v, evaluated at u. With this notation, the coarse grid solution $u_{H,P}$ is computed in the same manner, cf. (16); the resulting (alternative) two grid approximation $\tilde{u}_{2G} \in V(\mathcal{T}_h, \boldsymbol{p})$ is then defined as follows: find $\tilde{u}_{2G} \in V(\mathcal{T}_h, \boldsymbol{p})$ such that

$$N'_{h,p}[u_{H,P}](\tilde{u}_{2G}, v_{h,p}) = N'_{h,p}[u_{H,P}](u_{H,P}, v_{h,p}) - A_{h,p}(u_{H,P}, v_{h,p}) + F_{h,p}(v_{h,p}) \tag{26}$$

for all $v_{h,p} \in V(\mathcal{T}_h, \boldsymbol{p})$, cf. [3, 32], for example. Exploiting this alternative two-grid IP DGFEM, the second term on the right-hand side of (20) (for uniform orders $p_\kappa = p \geq 1$, $P_\kappa = P \geq 1$ $S_\kappa = S$, $1 \leq S \leq \min(P+1, K)$, $K \geq 1$, $h = \max_{\kappa \in \mathcal{T}_h} h_\kappa$, and $H = \max_{\kappa \in \mathcal{T}_H} H_\kappa$, with $\theta = 0$) is replaced by

$$\frac{p^7}{h^2} \frac{H^{4S-4}}{P^{4K-6}} \|u\|^4_{H^K(\Omega)}; \tag{27}$$

see [9] for details. We remark that this bound is rather pessimistic with respect to the polynomial degree, due to the exploitation of inverse inequalities in the analysis. A key disadvantage of this alternative two-grid IP DGFEM is that the statement and analysis of this method requires stricter regularity assumptions on μ. Indeed, the definition of the numerical scheme in (26) requires $\mu \in \mathrm{C}^1(\bar{\Omega} \times [0, \infty))$, while the underlying *a priori* error analysis, cf. (27), assumes that $\mu \in \mathrm{C}^2(\bar{\Omega} \times [0, \infty))$; these regularity assumptions may be unrealistic in applications, cf. [3]. With this in mind, we proceed in the next section to consider the *a posteriori* error estimation of the two-grid IP DGFEM (16)–(17).

3.2 *A Posteriori* Error Bound

In this section, we develop the *a posteriori* error analysis of the two-grid IP DGFEM defined by (16)–(17).

Let us denote by Π_{κ,p_κ} the L_2-projection onto $V(\mathcal{T}_h, \boldsymbol{p})$. Then, we state the following upper bound.

Theorem 3.2 *Let $u \in \mathrm{H}_0^1(\Omega)$ be the analytical solution of (5)–(6), $u_{H,P} \in V(\mathcal{T}_H, \boldsymbol{P})$ the numerical approximation obtained from (16) and $u_{2G} \in V(\mathcal{T}_h, \boldsymbol{p})$ the numerical approximation computed from (17); then the following hp-*a posteriori *error bound holds*

$$\|u - u_{2G}\|_{h,p} \leq C_5 \left(\sum_{\kappa \in \mathcal{T}_h} \left(\eta_\kappa^2 + \xi_\kappa^2 \right) + \sum_{\kappa \in \mathcal{T}_h} h_\kappa^2 p_\kappa^{-2} \| f - \Pi_{\kappa,p_\kappa} f \|_{\mathrm{L}_2(\kappa)}^2 \right)^{\frac{1}{2}}, \tag{28}$$

with a constant $C_5 > 0$, which is independent of h, H, $\boldsymbol{p}$ and $\boldsymbol{P}$. Here, for $\kappa \in \mathcal{T}_h$, the local fine grid error indicators η_κ *are defined by*

$$\begin{aligned} \eta_\kappa^2 &= h_\kappa^2 p_\kappa^{-2} \left\| \Pi_{\kappa,p_\kappa} f + \nabla \cdot \{ \mu(|\nabla u_{H,P}|) \nabla u_{2G} \} \right\|_{\mathrm{L}_2(\kappa)}^2 \\ &\quad + h_e p_e^{-1} \left\| [\![\mu(|\nabla u_{H,P}|) \nabla u_{2G}]\!] \right\|_{\mathrm{L}_2(\partial\kappa \setminus \Gamma)}^2 + \gamma^2 h_e^{-1} p_e^3 \| [\![u_{2G}]\!] \|_{\mathrm{L}_2(\partial\kappa)}^2, \end{aligned} \tag{29}$$

and the local two-grid error indicators ξ_κ *are defined, for all $\kappa \in \mathcal{T}_h$, as*

$$\xi_\kappa^2 = \left\| (\mu(|\nabla u_{H,P}|) - \mu(|\nabla u_{2G}|)) \nabla u_{2G} \right\|_{\mathrm{L}_2(\kappa)}^2. \tag{30}$$

Remark 3.4 We refer to η_κ as the local fine grid error indicators, since they are analogous to the corresponding error indicators present in the *a posteriori* error bounds derived for the standard IP DGFEM applied to both quasilinear problems and the linear Poisson problem, cf. [14, 16], respectively. On the other hand, the local error indicators ξ_κ stem from the exploitation of the two-grid approach. With this in mind, we refer to ξ_κ as the local two-grid error indicators; they effectively model the error generated by approximating the nonlinearity on the fine grid with the coarse grid solution.

Remark 3.5 We note that the third term in the local two-grid error indicator η_κ defined in (29) is sub-optimal with respect to the polynomial degree. This sub-optimality results from the fact that due to the possible presence of hanging nodes in $\mathcal{T}_h$, a non-conforming interpolant is used in the proof to Theorem 3.2. For conforming meshes, a conforming *hp*-version interpolant may be employed which removes this sub-optimality; see [16, Remark 3.3] for details.

Remark 3.6 In the case of an inhomogeneous boundary condition $u = g$ on Γ, the third term in the local error indicators η_κ is replaced by

$$\gamma^2 h_e^{-1} p_e^3 \| [\![u_{2G}]\!] \|_{\mathrm{L}_2(\partial\kappa \setminus \Gamma)}^2 + \gamma^2 h_e^{-1} p_e^3 \| u_{2G} - g_h \|_{\mathrm{L}_2(\partial\kappa \cap \Gamma)}^2,$$

where g_h is a piecewise approximation to the boundary function g; in this setting additional data-oscillation terms also arise, see [14] for details.

Remark 3.7 We remark that local lower bounds for the right-hand side of (28), i.e., the efficiency of the proposed error indicator, can be proved by adding the term

$$E^2 := \sum_{\kappa \in \mathcal{T}_h} \| \mu(|\nabla u|) \nabla u - \mu(|\nabla u_{H,P}|) \nabla u_{2G} \|_{\mathrm{L}_2(\kappa)}^2$$

to the norm $\|u - u_{2G}\|_{h,p}^2$. Then, by applying (8) we have

$$E^2 \leq 2 \sum_{\kappa \in \mathcal{T}_h} \xi_\kappa^2 + 2 \sum_{\kappa \in \mathcal{T}_h} \| \mu(|\nabla u|) \nabla u - \mu(|\nabla u_{2G}|) \nabla u_{2G} \|_{\mathrm{L}_2(\kappa)}^2$$

$$\leq 2\sum_{\kappa\in\mathcal{T}_h}\xi_\kappa^2 + 2C_1^2\sum_{\kappa\in\mathcal{T}_h}\|\nabla u-\nabla u_{2G}\|^2_{\mathrm{L}_2(\kappa)}$$

$$\leq 2\sum_{\kappa\in\mathcal{T}_h}\xi_\kappa^2 + 2C_1^2\|u-u_{2G}\|^2_{h,p},$$

and therefore we obtain (28) with the left-hand side being replaced by $(\|u-u_{2G}\|^2_{h,p}+E^2)^{\frac{1}{2}}$, and a different constant $\widetilde{C}_5$. Furthermore, in order to obtain lower bounds on the error, the fine grid indicators η_κ can be estimated in terms of the local error by proceeding along the lines of [16]. Finally, in order to bound the two-grid error indicators, we use again (8) to infer that

$$\begin{aligned}\xi_\kappa &\leq \left\|\mu(|\nabla u_{H,P}|)\nabla u_{2G}-\mu(|\nabla u|)\nabla u\right\|_{\mathrm{L}_2(\kappa)} + \|\mu(|\nabla u|)\nabla u-\mu(|\nabla u_{2G}|)\nabla u_{2G}\|_{\mathrm{L}_2(\kappa)}\\ &\leq \left\|\mu(|\nabla u_{H,P}|)\nabla u_{2G}-\mu(|\nabla u|)\nabla u\right\|_{\mathrm{L}_2(\kappa)} + C_1\,\|\nabla u-\nabla u_{2G}\|_{\mathrm{L}_2(\kappa)}\,.\end{aligned}$$

Remark 3.8 Based on the *hp-a posteriori* error analysis developed in [33], the error bound stated in Theorem 3.2 may be generalised to domains $\Omega\subset\mathbb{R}^3$, assuming that the underlying mesh $\mathcal{T}_h$ consists of 1-irregular hexahedral elements.

Proof of Theorem 3.2 The proof of this error bound is based on a generalisation of the proof of the corresponding *a posteriori* bound for the standard *hp*-version IP DGFEM for second-order quasilinear elliptic PDEs; see [16] for details. Given that the fine mesh partition $\mathcal{T}_h$ of Ω may contain hanging nodes, under the assumption that $\mathcal{T}_h$ is regularly reducible, i.e., $\mathcal{T}_h$ may be refined to create a conforming mesh $\mathcal{T}_{\widetilde{h}}$ as outlined in Sect. 2.1. We denote by $V(\mathcal{T}_{\widetilde{h}},\widetilde{\boldsymbol{p}})$ the corresponding DGFEM finite element space with polynomial degree vector $\widetilde{\boldsymbol{p}}$ defined by $\widetilde{p}_{\widetilde{\kappa}}=p_\kappa$ for any $\widetilde{\kappa}\in\mathcal{T}_{\widetilde{h}}$ with $\widetilde{\kappa}\subseteq\kappa$ and some $\kappa\in\mathcal{T}_h$. We note that $V(\mathcal{T}_h,\boldsymbol{p})\subseteq V(\mathcal{T}_{\widetilde{h}},\widetilde{\boldsymbol{p}})$ and due to the assumptions in Sect. 2.1, the DGFEM norms $\|\cdot\|_{h,p}$ and $\|\cdot\|_{\widetilde{h},\widetilde{p}}$ corresponding to the spaces $V(\mathcal{T}_h,\boldsymbol{p})$ and $V(\mathcal{T}_{\widetilde{h}},\widetilde{\boldsymbol{p}})$, respectively, are equivalent on $V(\mathcal{T}_h,\boldsymbol{p})$, cf. [16].

An important step in our analysis is the decomposition of the DGFEM space $V(\mathcal{T}_{\widetilde{h}},\widetilde{\boldsymbol{p}})$ into two orthogonal subspaces, cf. [17]: a conforming part $[V(\mathcal{T}_{\widetilde{h}},\widetilde{\boldsymbol{p}})]^{\|}=V(\mathcal{T}_{\widetilde{h}},\widetilde{\boldsymbol{p}})\cap\mathrm{H}^1_0(\Omega)$, and a nonconforming part $[V(\mathcal{T}_{\widetilde{h}},\widetilde{\boldsymbol{p}})]^{\perp}$ defined as the orthogonal complement of $[V(\mathcal{T}_{\widetilde{h}},\widetilde{\boldsymbol{p}})]^{\|}$ in $V(\mathcal{T}_{\widetilde{h}},\widetilde{\boldsymbol{p}})$ with respect to the DGFEM energy inner product $(\cdot,\cdot)_{\widetilde{h},\widetilde{p}}$ (inducing the DGFEM energy norm $\|\cdot\|_{\widetilde{h},\widetilde{p}}$), i.e.,

$$V(\mathcal{T}_{\widetilde{h}},\widetilde{\boldsymbol{p}})=[V(\mathcal{T}_{\widetilde{h}},\widetilde{\boldsymbol{p}})]^{\|}\oplus_{\|\cdot\|_{\widetilde{h},\widetilde{p}}}[V(\mathcal{T}_{\widetilde{h}},\widetilde{\boldsymbol{p}})]^{\perp}.$$

Based on this setting, the DGFEM-solution u_{2G} obtained by (16)–(17) may be split accordingly,

$$u_{2G}=u_{2G}^{\|}+u_{2G}^{\perp}, \tag{31}$$

where $u_{2G}^{\|}\in[V(\mathcal{T}_{\widetilde{h}},\widetilde{\boldsymbol{p}})]^{\|}$ and $u_{2G}^{\perp}\in[V(\mathcal{T}_{\widetilde{h}},\widetilde{\boldsymbol{p}})]^{\perp}$. We can define the error in the solution obtained by (16)–(17) as

$$E_{h,p}=u-u_{2G}, \tag{32}$$

and let

$$E_{h,p}^{\|}=u-u_{2G}^{\|}\in\mathrm{H}^1_0(\Omega). \tag{33}$$

We notice that

$$\left\| E_{h,p}^{\parallel} \right\|_{h,p} \leq C_{\mathrm{D}} \left\| E_{h,p} \right\|_{h,p}, \tag{34}$$

where the constant $C_{\mathrm{D}} > 0$ is independent of γ, h and $\boldsymbol{p}$ but depends only on the shape regularity of $\mathcal{T}_h$ and the constants ρ_1 and ρ_2 in (11) and (12), respectively; see [16, Corollary 3.6].

Exploiting inequality (9) yields

$$\begin{aligned} C_2 \left\| E_{h,p} \right\|_{h,p}^2 &= C_2 \left(\sum_{\widetilde{\kappa} \in \mathcal{T}_{\widetilde{h}}} \int_{\widetilde{\kappa}} |\nabla u - \nabla u_{2G}|^2 \,\mathrm{d}\boldsymbol{x} + \sum_{e \in \mathcal{E}_h} \int_e \sigma_{h,p} |[\![E_{h,p}]\!]|^2 \,\mathrm{d}s \right) \\ &\leq \sum_{\widetilde{\kappa} \in \mathcal{T}_{\widetilde{h}}} \int_{\widetilde{\kappa}} \{ \mu(|\nabla u|) \nabla u - \mu(|\nabla u_{2G}|) \nabla u_{2G} \} \cdot \nabla E_{h,p} \,\mathrm{d}\boldsymbol{x} \\ &\quad + C_2 \sum_{e \in \mathcal{E}_h} \int_e \sigma_{h,p} |[\![E_{h,p}]\!]|^2 \,\mathrm{d}s. \end{aligned}$$

Here, we point out that the volume integrals appearing in the above equation are defined over the conforming mesh $\mathcal{T}_{\widetilde{h}}$, while the edge integral terms are defined over the skeleton of the original (fine) mesh $\mathcal{T}_h$, cf. [16]. By noticing that $E_{h,p} = E_{h,p}^{\parallel} - u_{2G}^{\perp}$, we split the right-hand side of this inequality into the following four parts

$$C_2 \left\| E_{h,p} \right\|_{h,p}^2 \leq |T_1| + |T_2| + |T_3| + |T_4|, \tag{35}$$

where

$$\begin{aligned} T_1 &= \sum_{\widetilde{\kappa} \in \mathcal{T}_{\widetilde{h}}} \int_{\widetilde{\kappa}} \left\{ \mu(|\nabla u|) \nabla u - \mu(|\nabla u_{H,P}|) \nabla u_{2G} \right\} \cdot \nabla E_{h,p}^{\parallel} \,\mathrm{d}\boldsymbol{x}, \\ T_2 &= - \sum_{\widetilde{\kappa} \in \mathcal{T}_{\widetilde{h}}} \int_{\widetilde{\kappa}} \{ \mu(|\nabla u|) \nabla u - \mu(|\nabla u_{2G}|) \nabla u_{2G} \} \cdot \nabla u_{2G}^{\perp} \,\mathrm{d}\boldsymbol{x}, \\ T_3 &= C_2 \sum_{e \in \mathcal{E}_h} \int_e \sigma_{h,p} |[\![E_{h,p}]\!]|^2 \,\mathrm{d}s, \\ T_4 &= \sum_{\widetilde{\kappa} \in \mathcal{T}_{\widetilde{h}}} \int_{\widetilde{\kappa}} \left\{ \mu(|\nabla u_{H,P}|) \nabla u_{2G} - \mu(|\nabla u_{2G}|) \nabla u_{2G} \right\} \cdot \nabla E_{h,p}^{\parallel} \,\mathrm{d}\boldsymbol{x}. \end{aligned}$$

Here, $E_{h,p}^{\parallel} \in \mathrm{H}_0^1(\Omega)$ and $u_{2G}^{\perp} \in [V(\mathcal{T}_h, \boldsymbol{p})]^{\perp}$ are defined by (33) and (31), respectively. We note that T_1, T_2 and T_3 are analogous to the corresponding terms which arise in the *a posteriori* error analysis of the standard IP DGFEM discretisation of (5)–(6), cf. [8] and [16]. Indeed, from [8] and [16], we recall the following bound:

$$|T_1| + |T_2| + |T_3| \leq C \left(\sum_{\kappa \in \mathcal{T}_h} \eta_\kappa^2 \right)^{\frac{1}{2}} \left\| E_{h,p} \right\|_{h,p}, \tag{36}$$

noting that the constant C depends on the constants m_μ, M_μ, C_1 and C_2 resulting from the monotonicity of μ, cf. (7). We now consider the term T_4:

$$\begin{aligned} T_4 &= \sum_{\widetilde{\kappa}\in\mathcal{T}_{\widetilde{h}}} \int_{\widetilde{\kappa}} \left\{\mu(|\nabla u_{H,P}|)\nabla u_{2G} - \mu(|\nabla u_{2G}|)\nabla u_{2G}\right\} \cdot \nabla E^{\parallel}_{h,p}\,\mathrm{d}\boldsymbol{x} \\ &= \sum_{\kappa\in\mathcal{T}_h} \int_{\kappa} \left\{\mu(|\nabla u_{H,P}|)\nabla u_{2G} - \mu(|\nabla u_{2G}|)\nabla u_{2G}\right\} \cdot \nabla E^{\parallel}_{h,p}\,\mathrm{d}\boldsymbol{x} \\ &\le \sum_{\kappa\in\mathcal{T}_h} \left\|(\mu(|\nabla u_{H,P}|) - \mu(|\nabla u_{2G}|))\nabla u_{2G}\right\|_{\mathrm{L}_2(\kappa)} \left\|\nabla E^{\parallel}_{h,p}\right\|_{\mathrm{L}_2(\kappa)} \\ &\le \left(\sum_{\kappa\in\mathcal{T}_h} \xi_\kappa^2\right)^{\frac{1}{2}} \left\|E^{\parallel}_{h,p}\right\|_{h,p}. \end{aligned}$$

Thereby, applying (34), gives

$$T_4 \le C_{\mathrm{D}} \left(\sum_{\kappa\in\mathcal{T}_h} \xi_\kappa^2\right)^{\frac{1}{2}} \left\|E_{h,p}\right\|_{h,p}. \tag{37}$$

Inserting (36) and (37) into (35) gives

$$C_2 \left\|E_{h,p}\right\|^2_{h,p} \le C \left(\sum_{\kappa\in\mathcal{T}_h} \eta_\kappa^2\right)^{\frac{1}{2}} \left\|E_{h,p}\right\|_{h,p} + C_{\mathrm{D}} \left(\sum_{\kappa\in\mathcal{T}_h} \xi_\kappa^2\right)^{\frac{1}{2}} \left\|E_{h,p}\right\|_{h,p}.$$

Dividing both sides of the above inequality by $\|E_{h,p}\|_{h,p}$, using the Cauchy–Schwarz inequality, and applying the triangle inequality in order to replace f by $\Pi_{\kappa,p_\kappa} f$, completes the proof of Theorem 3.2. □

4 Two-Grid *hp*-Adaptive Mesh Refinement Algorithm

For the standard IP DGFEM discretisation of the quasilinear problem (5)–(6), the mesh may be automatically constructed using the *hp*-adaptive refinement algorithm outlined in [16]. In that setting, the local error indicators are defined in an analogous way to η_κ given in (29), with $u_{H,P}$ and u_{2G} both replaced by $u_{h,p}$. In the context of the two-grid IP DGFEM discretisation defined by (16)–(17), it is necessary to refine both the fine and coarse meshes, together with their corresponding polynomial degree vectors, in order to decrease the error between u and u_{2G} with respect to the energy norm $\|\cdot\|_{h,p}$.

To this end, we first note that, from Theorem 3.2, we have, for each fine element $\kappa \in \mathcal{T}_h$, a local error indicator η_κ and a local two-grid error indicator ξ_κ. As noted above, the local error indicator η_κ is similar to the one which arises within the analysis of the standard IP DGFEM discretisation. With this in mind, η_κ represents the error arising from the linear fine grid solve defined in (17), while the local two-grid error indicator ξ_κ represents the error stemming from the approximation of the nonlinear coefficient $\mu(|\nabla u_{h,p}|)$ on the fine mesh $\mathcal{T}_h$ by the same quantity evaluated with respect to the coarse grid solution $u_{H,P}$, i.e., the error committed by replacing $\mu(|\nabla u_{h,p}|)$ by $\mu(|\nabla u_{H,P}|)$.

With this observation, we design the fine finite element space $V(\mathcal{T}_h, \boldsymbol{p})$ by employing the local error indicators (29), while the coarse finite element space $V(\mathcal{T}_H, \boldsymbol{P})$ is constructed in such a manner as to control the size of the local two-grid error indicators (30). More precisely, we wish to design both $V(\mathcal{T}_h, \boldsymbol{p})$ and $V(\mathcal{T}_H, \boldsymbol{P})$ in such a manner that η_κ and ξ_κ are of comparable size. To this end, we propose the following algorithm.

Algorithm 4.1 The finite element spaces $V(\mathcal{T}_h, \boldsymbol{p})$ and $V(\mathcal{T}_H, \boldsymbol{P})$ are constructed, based on employing the following algorithm.

1. Initial step: Select initial coarse and fine meshes $\mathcal{T}_H$ and $\mathcal{T}_h$, as well as initial coarse and fine polynomial degree distributions $\boldsymbol{P}$ and $\boldsymbol{p}$, respectively, in such a manner that the resulting coarse and fine *hp*-finite element spaces $V(\mathcal{T}_H, \boldsymbol{P})$ and $V(\mathcal{T}_h, \boldsymbol{p})$, respectively, satisfy the condition: $V(\mathcal{T}_H, \boldsymbol{P}) \subseteq V(\mathcal{T}_h, \boldsymbol{p})$.
2. Perform *hp*-mesh refinement of the fine *hp*-finite element space $V(\mathcal{T}_h, \boldsymbol{p})$: more precisely, using the fine grid error indicators η_κ from (29), apply a fixed fraction strategy to mark elements with a comparatively large error contribution. Then, if an element is set for refinement, decide on whether to perform h- or p-refinement based on testing the smoothness of the fine grid solution u_{2G}; see, e.g., [15] (or [27]) to design $V(\mathcal{T}_h, \boldsymbol{p})$.
3. Perform coarse mesh refinement: for a fixed constant steering parameter $0 \leq \lambda < \infty$, for each element $\kappa \in \mathcal{T}_h$, do:
   (a) If $\lambda \xi_\kappa^2 \geq \eta_\kappa^2$ then mark for refinement the coarse element $\kappa_H \in \mathcal{T}_H$ where $\kappa \subseteq \kappa_H$.
   (b) If the element is set for refinement decide on whether to perform h- or p-refinement, e.g., by again testing the smoothness of the coarse grid solution $u_{H,P}$; see, [15, Sect. 2.4.1] (or [27]).
4. Perform mesh smoothing to ensure:

   - For all fine elements $\kappa \in \mathcal{T}_h$ there exists a coarse mesh element $\kappa_H \in \mathcal{T}_H$ such that $\kappa \subseteq \kappa_H$;
   - For all $\kappa \in \mathcal{T}_h$ and $\kappa_H \in \mathcal{T}_H$, where $\kappa \subseteq \kappa_H$, that $P_\kappa \leq p_\kappa$.

   In this article we perform h-refinement on the fine mesh $\mathcal{T}_h$ and p-derefinement on the coarse mesh $\mathcal{T}_H$ where necessary.

Remark 4.1 For the purposes of the numerical experiments in the following section, we start the two-grid *hp*-adaptive algorithm with $V(\mathcal{T}_H, \boldsymbol{P}) = V(\mathcal{T}_h, \boldsymbol{p})$ in Step 1 above.

Remark 4.2 We note that the algorithm allows the steering parameter λ to be zero. In this situation no coarse mesh refinement will be performed and hence the algorithm will only refine the fine mesh.

5 Numerical Experiments

In this section we present a series of numerical experiments in two- and three-dimensional space to demonstrate the performance of the *a posteriori* error bound derived in Theorem 3.2 and the *hp*-adaptive mesh refinement strategy from Algorithm 4.1. We set the interior penalty parameter constant γ to 10 and the steering parameter λ to 1 for all experiments. The nonlinear equations are solved by employing a damped Newton method [21, Sect. 14.4]. The solution of the resulting set of linear equations, emanating from either the fine mesh or at each step of the iterative nonlinear solver, was computed using either the direct MUMPs

solver, see [1], for two-dimensional problems or an ILU preconditioned GMRES algorithm, see [23], for the three-dimensional problem. We also calculate the error bound stated in Theorem 3.2, cf. (28), by setting the constant C_5 equal to 1.

For each example, as well as solving using the two-grid method, we compute the standard IP DGFEM formulation (14) for comparison. In order to determine the improvement in the computation time from using the two-grid method over the standard IP DGFEM, both algorithms were timed, on the same computer, using the FORTRAN `CPU_time` function [20, Sect. 8.16.2], which times purely the amount of CPU time and is therefore unaffected by other processes on the computer.

Example 1 In this example we repeat the first numerical experiment from [16, Sect. 4.1]. Therefore, we let Ω be the unit square $(0,1)^2 \subset \mathbb{R}^2$ and define the nonlinear coefficient as

$$\mu(\boldsymbol{x}, |\nabla u|) = 2 + \frac{1}{1+|\nabla u|}. \tag{38}$$

We select the right-hand forcing function f so that the analytical solution to (5)–(6) is given by

$$u(x,y) = x(1-x)y(1-y)(1-2y)\mathrm{e}^{-20(2x-1)^2}.$$

In Fig. 1(a) we present a comparison of the actual error measured in terms of the energy norm versus the third root of the number of degrees of freedom (of the fine mesh) for both the standard DGFEM formulation (14), together with the two-grid IP DGFEM (16)–(17). In this figure we perform both h- and hp-adaptive mesh refinement for both schemes. Here, we can see that, for the problem at hand, the true error in the two-grid IP DGFEM is only marginally worse than the corresponding quantity for the standard IP DGFEM, when the same number of degrees of freedom in the two-grid fine mesh, as in the mesh for the standard IP DGFEM, are used. From Fig. 1(b), we observe that for both the h- and hp-refinement strategy, the error bound overestimates the true error by a roughly consistent amount, in the sense that the effectivity indices are roughly constant; indeed, here, the effectivity indices are around 13. Although the two-grid IP DGFEM gives a slightly worse error than the standard IP DGFEM, for a fixed number of fine mesh degrees of freedom, we note that the two-grid algorithm only performs the expensive nonlinear solve on a coarser grid which, hopefully, possesses far less degrees of freedom than the standard IP DGFEM. Therefore, in Fig. 1(c) we compare, at each iteration of the automatic two-grid mesh refinement algorithm, the number of degrees of freedom used in both the coarse and fine finite element spaces. As can be seen, there are considerable less degrees of freedom on the coarse grid and, therefore, we would expect the two-grid solver to be computationally less expensive. To this end, the magnitude of the true error, measured in the DGFEM norm, for both the standard and two-grid methods, when both h- and hp-adaptive mesh refinement has been employed, compared to the cumulative CPU time required for the calculation of each numerical solution is shown in Fig. 2. This figure clearly illustrates the superiority of employing the two-grid variant of the IP DGFEM for this problem. Indeed, for a given fixed accuracy, the two-grid IP DGFEM requires around an order of magnitude less CPU time to compute the numerical approximation to u, compared to the standard IP DGFEM.

In Fig. 3 we show the fine and coarse h- and hp-refinement meshes after 11 mesh refinements, where the colour bar indicates the polynomial degree for hp-refinement. For h-refinement we can see that all the fine grid refinement occurs around the interior and bases of the exponential 'hills' in the analytical solution, as would occur for the standard IP

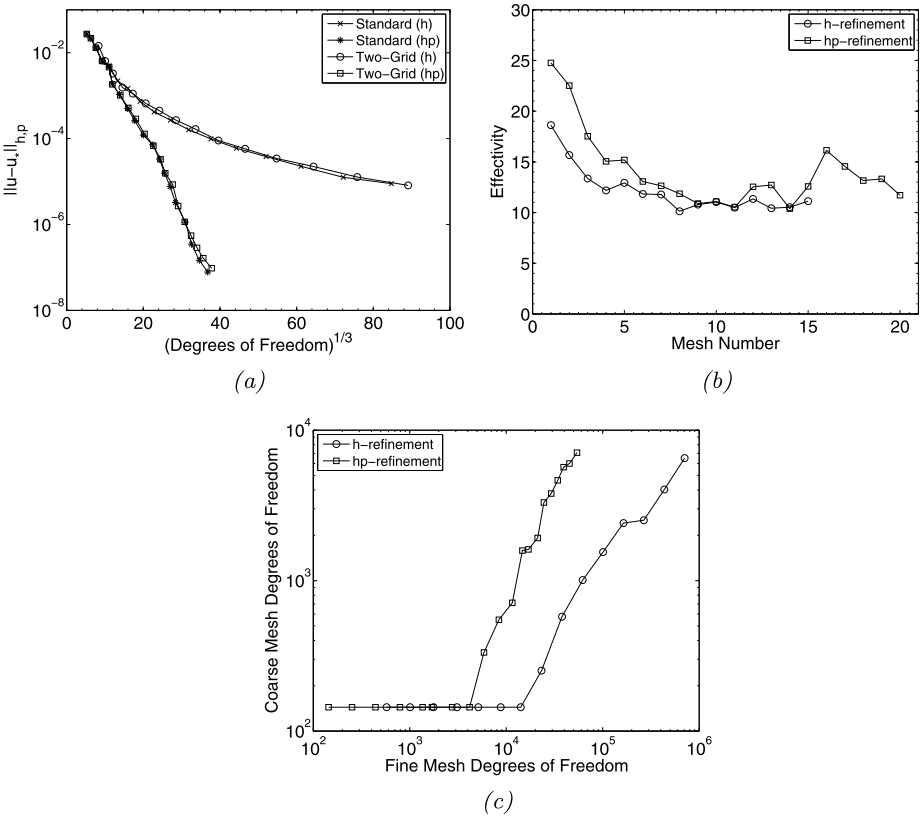

Fig. 1 Example 1. (**a**) Comparison of the error in the DGFEM norm, using both the standard nonlinear solver ($u_* = u_{h,p}$) and the two-grid method ($u_* = u_{2G}$), with respect to the number of degrees of freedom; (**b**) Effectivity of the h- and hp-refinement using the two-grid method; (**c**) Comparison of number of degrees of freedom in the coarse and fine mesh at each iteration of the automatic mesh refinement algorithm

DGFEM. Notice that only a small amount of refinement has taken place in the corresponding elements in the coarse mesh, namely, wherever ξ_κ is expected to be large. In the fine mesh of the hp-refinement case the h-refinement occurs mostly around the base of the hills with p-refinement in the interior of the hills, cf. also the coarse grid.

Example 2 In this example we repeat the second numerical experiment from [16, Sect. 4.2]. Thereby, we let Ω denote the L-shaped domain $(-1,1)^2 \setminus [0,1) \times (-1,0] \subset \mathbb{R}^2$ and select the nonlinearity to be

$$\mu(\boldsymbol{x}, |\nabla u|) = 1 + \mathrm{e}^{-|\nabla u|^2}.$$

By writing (r, φ) to denote the system of polar coordinates, we choose the forcing function f and an inhomogeneous boundary condition such that the analytical solution to (5)–(6) is

$$u = r^{2/3} \sin\left(\frac{2}{3}\varphi\right).$$

Note that u is analytic in $\bar{\Omega} \setminus \{\mathbf{0}\}$, but ∇u is singular at the origin.

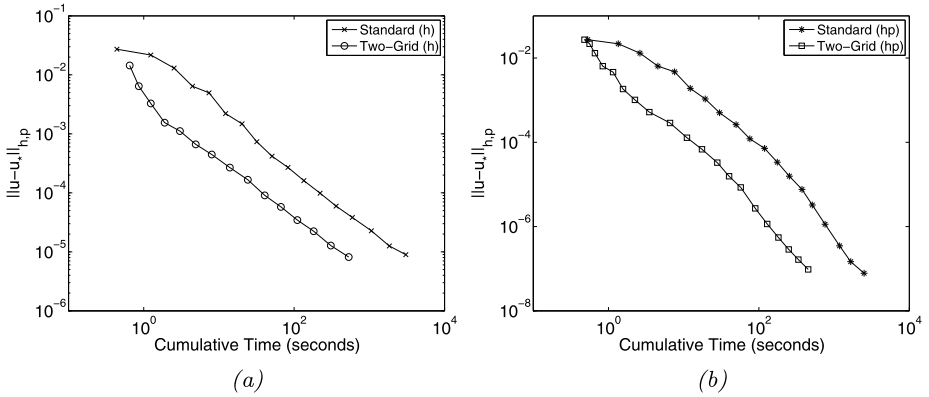

Fig. 2 Example 1. Cumulative CPU timing of the standard ($u_* = u_{h,p}$) and two-grid ($u_* = u_{2G}$) solver compared to the actual error in the DGFEM norm: (**a**) h-refinement; (**b**) hp-refinement

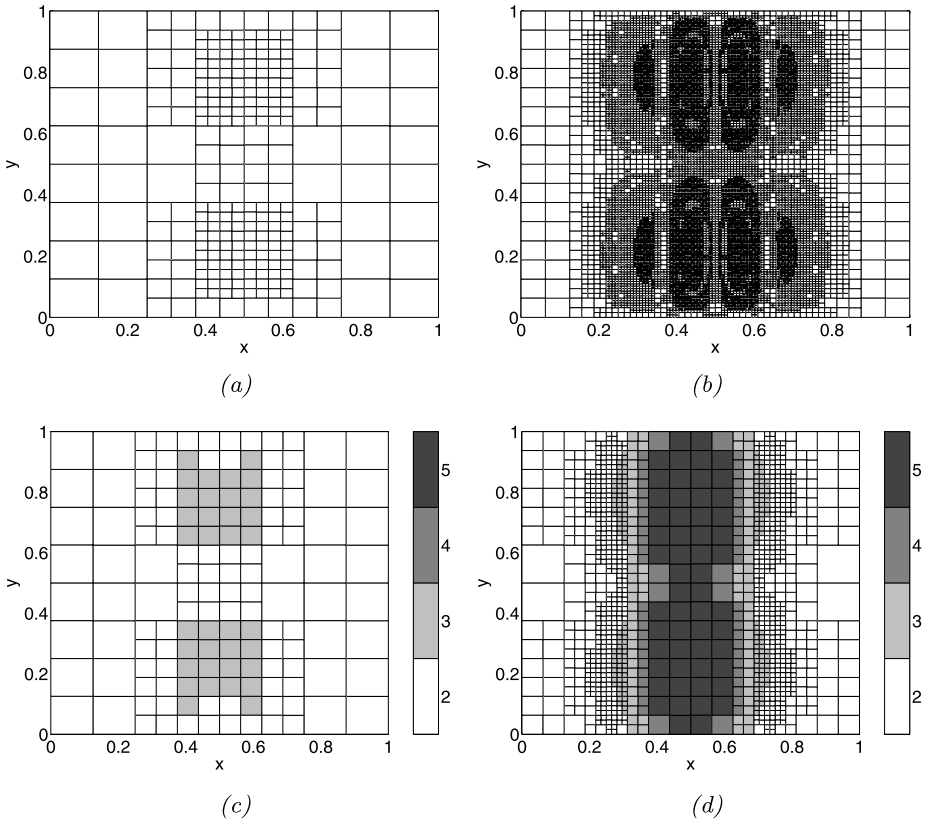

Fig. 3 Example 1. (**a**) Coarse and (**b**) fine meshes after 11 h-adaptive refinements; (**c**) Coarse and (**d**) fine meshes after 11 hp-adaptive refinements

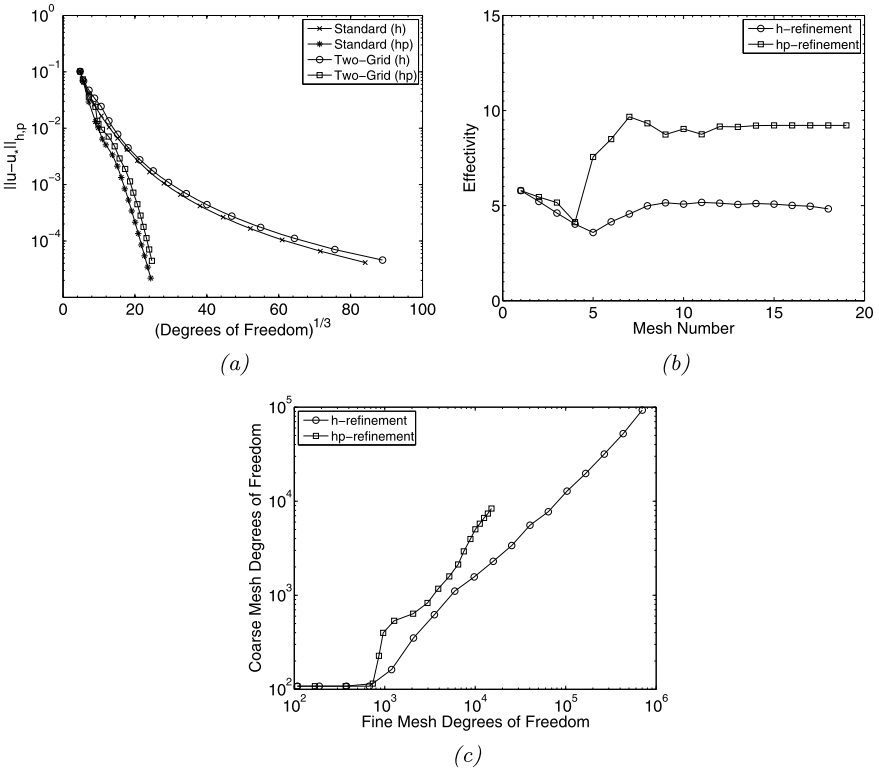

Fig. 4 Example 2. (**a**) Comparison of the error in the DGFEM norm, using both a standard nonlinear solver ($u_* = u_{h,p}$) and the two-grid method ($u_* = u_{2G}$), with respect to the number of degrees of freedom; (**b**) Effectivity of the h- and hp-refinement using the two-grid method; (**c**) Comparison of number of degrees of freedom in the coarse and fine mesh for each iteration of the automatic two-grid mesh refinement algorithm

In Fig. 4(a), we again present a comparison of the actual error measured in terms of the energy norm versus the third root of the number of degrees of freedom (of the fine mesh) for both the standard IP DGFEM formulation (14), together with the two-grid IP DGFEM (16)–(17), employing both h- and hp-refinement. As in Example 1, for this problem the true error in the two-grid IP DGFEM is only marginally worse than the corresponding quantity for the standard IP DGFEM, when the same number of degrees of freedom in the two-grid fine mesh, as in the mesh for the standard IP DGFEM, are employed. Figure 4(b), shows the effectivity indices of both the h- and hp-refinement strategies. For all meshes, these are roughly constant. We can see from Fig. 4(c), which shows the number of degrees of freedom on the coarse grid compared to the number of degrees of freedom on the fine mesh at each iteration of the automatic mesh refinement algorithm, that there are considerable less degrees of freedom on the coarse grid and, thereby, we would again expect the two-grid solver to be computationally less expensive. In Fig. 5 we plot the cumulative CPU time taken by the two schemes, which is compared to the actual error, for both h- and hp-refinement strategies. Here, we see that for h-refinement, the two-grid IP DGFEM results in an error that is roughly a constant amount lower than the error in the standard method, for the same computation time. For hp-refinement, we see that initially the two-grid method is less computationally expensive, however, as refinement proceeds the improvement in computation time from using the two-grid method decreases.

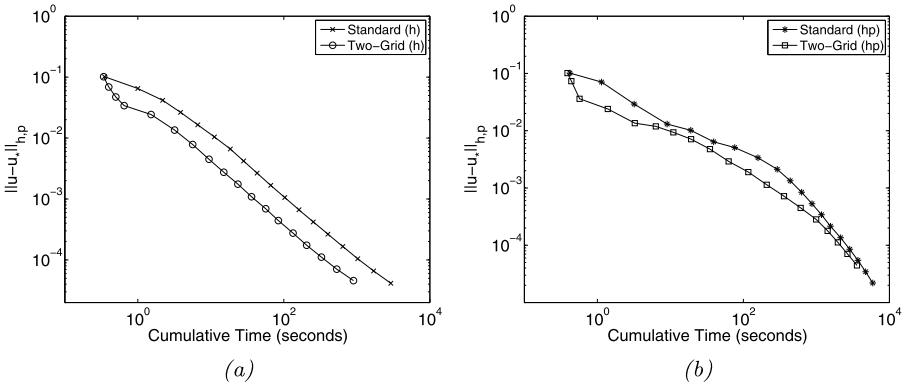

Fig. 5 Example 2. Cumulative CPU timing of the standard ($u_* = u_{h,p}$) and two-grid ($u_* = u_{2G}$) solver compared to the actual error in the DGFEM norm: (**a**) h-refinement; (**b**) hp-refinement

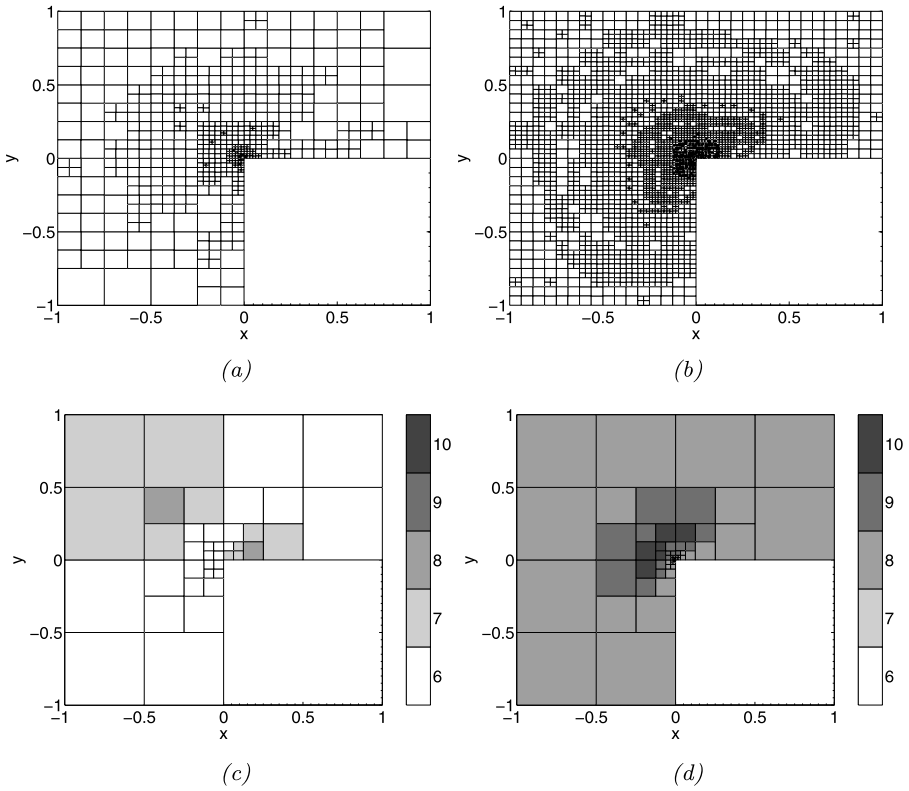

Fig. 6 Example 2. (**a**) Coarse and (**b**) fine meshes after 11 h-adaptive refinements; (**c**) Coarse and (**d**) fine meshes after 11 hp-adaptive refinements

In Fig. 6 we show the fine and coarse h- and hp-refinement meshes after 11 mesh refinements, where the colour bar indicates the polynomial degree for hp-refinement. For h-refinement we can see that both the fine and coarse grid refinement is fairly uniform

except around the singularity at the origin, where strong refinement appears, with the coarse grid mesh refinement being less refined. For the *hp*-refinement case, the *h*-refinement occurs mostly around the origin with high p-refinement in the rest of the domain, with the coarse grid refinement done mostly by p-refinement, with a small amount of *h*-refinement around the origin.

Example 3 In this section we let Ω be the Fichera corner $(-1,1)^3 \setminus [0,1)^3 \subset \mathbb{R}^3$, use the nonlinearity (38) from the first example and select f and a suitable inhomogeneous boundary conditions such that the analytical solution to (5)–(6) is

$$u(x,y,z) = (x^2+y^2+z^2)^{q/2},$$

where $q \in \mathbb{R}$. From [4] we note that for $q > -1/2$ the solution satisfies $u \in H^1(\Omega)$; in this case we select $q = -1/4$ as in [33]. We note that this gives a singularity at the re-entrant corner (the origin).

In Fig. 7(a), we again present a comparison of the actual error measured in terms of the energy norm versus the fourth root (see [33]) of the number of degrees of freedom (of the fine mesh) for both the standard IP DGFEM formulation (14), together with the two-grid

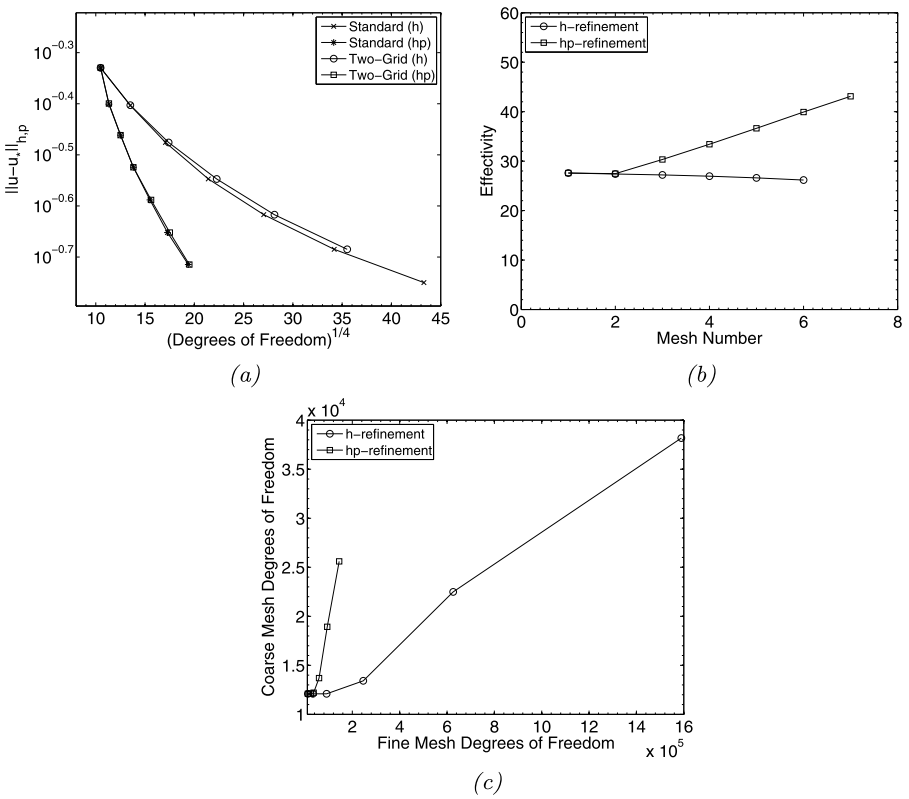

Fig. 7 Example 3. (**a**) Comparison of the error in the DGFEM norm, using both a standard nonlinear solver ($u_* = u_{h,p}$) and the two-grid method ($u_* = u_{2G}$), with respect to the number of degrees of freedom; (**b**) Effectivity of the *h*- and *hp*-refinement using the two-grid method; (**c**) Comparison of number of degrees of freedom in the coarse and fine mesh for each iteration of the automatic two-grid mesh refinement algorithm

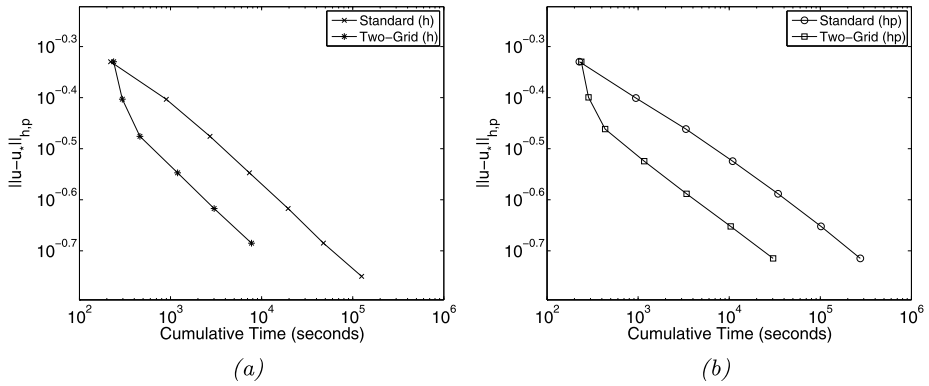

Fig. 8 Example 3. (**a**) Cumulative CPU timing of standard ($u_* = u_{h,p}$) and two-grid ($u_* = u_{2G}$) solver compared to the actual error in the DGFEM norm: (**a**) h-refinement; (**b**) hp-refinement

IP DGFEM (16)–(17), employing both h- and hp-refinement. Here, we can see that for this problem the true error in the two-grid IP DGFEM is almost identical to the corresponding quantity for the standard IP DGFEM when the same number of degrees of freedom in the two-grid fine mesh is employed as in the mesh for the standard IP DGFEM. From Fig. 7(b), we can see that the effectivity indices of the h-refinement strategy are roughly constant, suggesting that the error bound constantly overestimates the error. For the hp-refinement strategy, we note that the effectivity index seems to rise slightly as refinement occurs; we point out that similar behaviour was observed in [33] for the numerical approximation of the Poisson equation posed in the same Fichera corner domain. From Fig. 7(c), which shows the number of degrees of freedom on the coarse grid compared to the number of degrees of freedom on the fine mesh at each iteration of the automatic mesh refinement algorithm, we can see that the two-grid solver uses significantly less degrees of freedom on the coarse grid than on the fine mesh; thereby, we would expect the computation time to be considerable lower than for the standard solver. From the comparison of the cumulative CPU timing with the actual error in the DGFEM norm, Fig. 8, this expected improvement is indeed observed for both h- and hp-refinement strategies. In particular, for a given fixed accuracy, the two-grid IP DGFEM requires around an order of magnitude less CPU time to compute the numerical approximation to u, compared to the standard IP DGFEM.

Figure 9 shows the fine and coarse meshes after 5 h-refinements. We can see that both the fine and coarse grid refinement is fairly uniform but concentrated around the singularity at the origin; we also note that the coarse mesh is less refined than the fine mesh, as we would expect. The fine and coarse meshes after 6 hp-mesh refinements are shown in Fig. 10. Here, we see that at the singularity at the origin both the fine and coarse meshes have mostly h-refinement with p-refinement occurring away from this area. Again we can see that both the coarse and fine meshes have been refined in a similar manner, with the coarse mesh just being less refined than the fine mesh.

6 Concluding Remarks

In this article, we have developed the *a priori* and *a posteriori* error analysis for a class of two-grid hp-version IP DGFEMs for the numerical solution of second-order quasilinear elliptic boundary value problems of monotone type. In particular, due to the type of

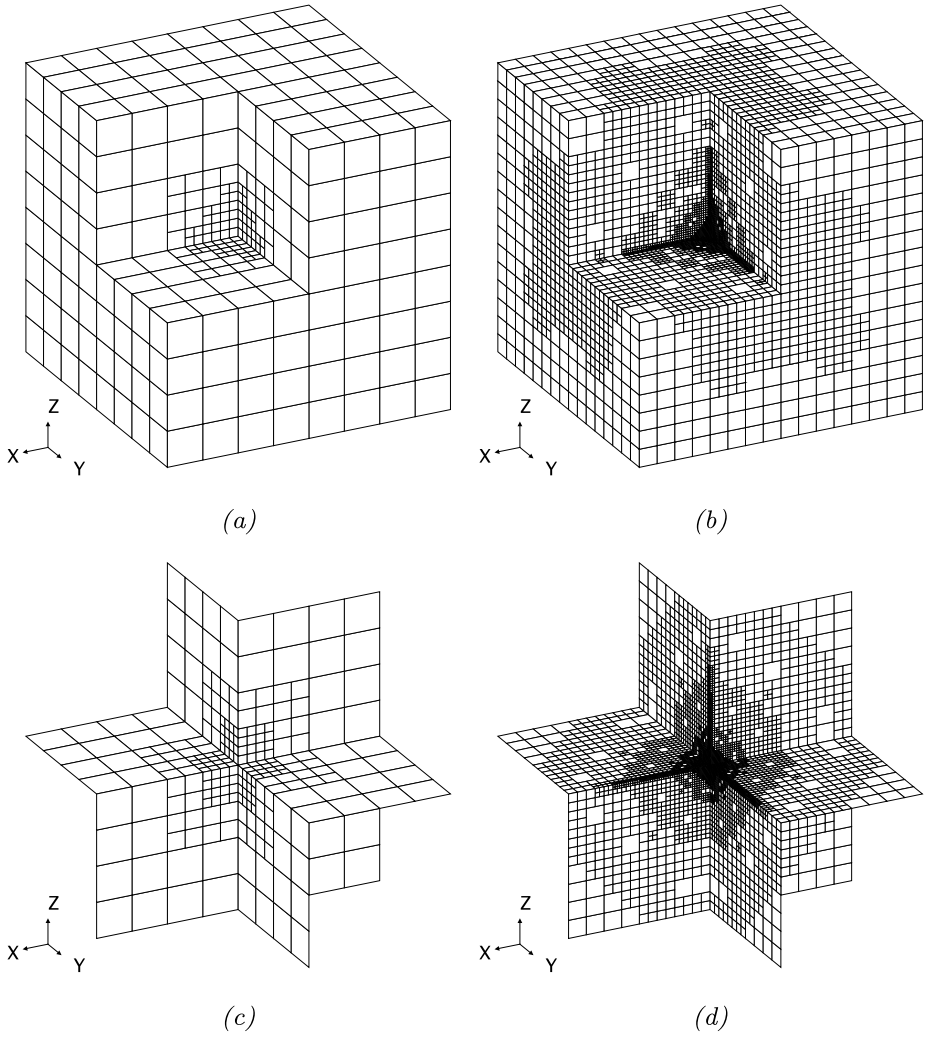

Fig. 9 Example 3. Finite element mesh after 5 h-adaptive mesh refinements: (**a**) Coarse mesh; (**b**) Fine mesh; (**c**) Three-slice of coarse mesh; (**d**) Three-slice of fine mesh

nonlinearity considered, the *a priori* error bounds indicate that the dimension of the coarse and fine finite element spaces $V(\mathcal{T}_H, \boldsymbol{P})$ and $V(\mathcal{T}_h, \boldsymbol{p})$, respectively, should grow at roughly the same rate, in order to retain optimal convergence of the underlying numerical method; computational results confirming these theoretical findings have been presented in [10]. On the basis of the *a posteriori* error bound, we have designed and implemented a two-grid *hp*-adaptive algorithm which is capable of designing both the coarse and fine finite element spaces $V(\mathcal{T}_H, \boldsymbol{P})$ and $V(\mathcal{T}_h, \boldsymbol{p})$, respectively, in an automatic manner. In particular, our numerical experiments indicate that gains in computational efficiency may be attained when the two-grid method is exploited in comparison to the standard (single grid) IP DGFEM; especially, the examples under consideration clearly show that, in spite of the *a priori* results suggesting an increase of the degrees of freedom in the fine and coarse finite element spaces

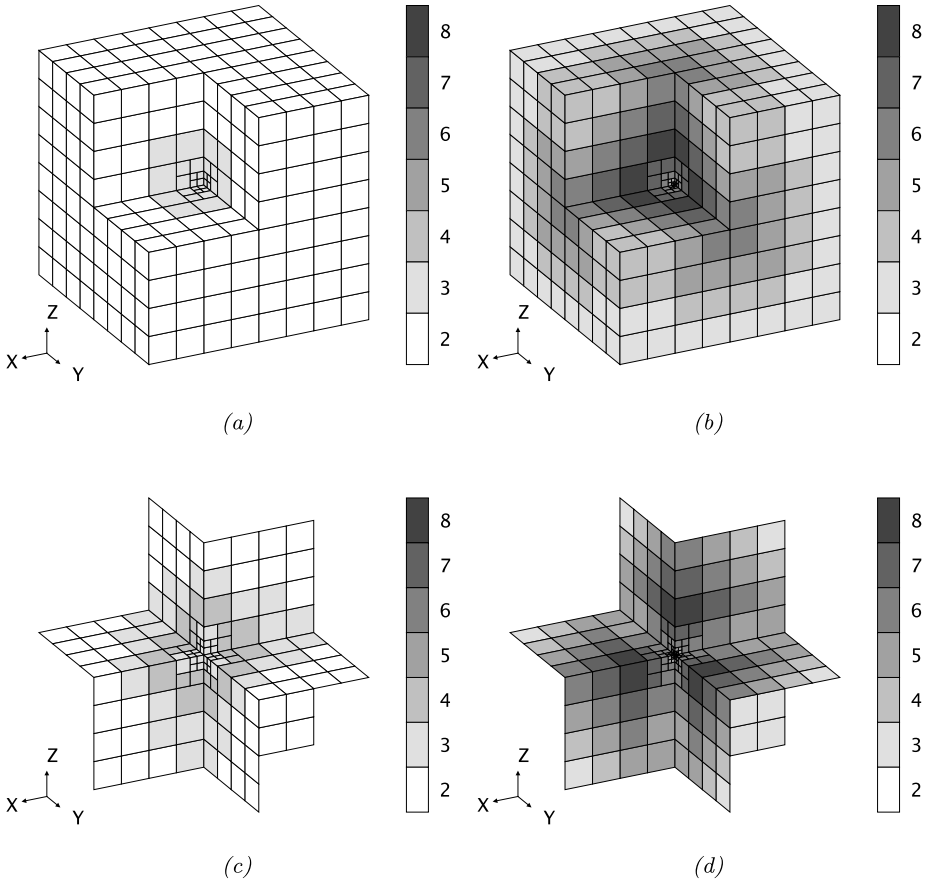

Fig. 10 Example 3. Finite element mesh after 6 *hp*-adaptive mesh refinements: (**a**) Coarse mesh; (**b**) Fine mesh; (**c**) Three-slice of coarse mesh; (**d**) Three-slice of fine mesh

at the same rate, there is a considerable difference when comparing the adaptive meshes on the coarse and on the fine scale. Current work is based on extending the present analysis to non-Newtonian fluid flows in both two- and three-dimensions, as well as to more complex nonlinear problems.

Acknowledgements PH acknowledges the financial support of the EPSRC under the grant EP/H005498. TW acknowledges the financial support of the Swiss National Science Foundation (SNF) under grant No. 200021126594.

References

1. Amestoy, P.R., Duff, I.S., L'Excellent, J.-Y.: Multifrontal parallel distributed symmetric and unsymmetric solvers. Comput. Methods Appl. Mech. Eng. **184**, 501–520 (2000)
2. Antonietti, P.F., Ayuso, B.: Schwarz domain decomposition preconditioners for discontinuous Galerkin approximations of elliptic problems: non-overlapping case. Math. Model. Numer. Anal. **41**(1), 21–54 (2007)
3. Axelsson, O., Layton, W.: A two-level method for the discretization of nonlinear boundary value problems. SIAM J. Numer. Anal. **33**(6), 2359–2374 (1996)

4. Beilina, L., Korotov, S., Křížek, M.: Nonobtuse tetrahedral partitions that refine locally towards Ficheralike corners. Appl. Math. **50**(6), 569–581 (2005)
5. Bi, C., Ginting, V.: Two-grid finite volume element method for linear and nonlinear elliptic problems. Numer. Math. **108**, 177–198 (2007)
6. Bi, C., Ginting, V.: Two-grid discontinuous Galerkin method for quasi-linear elliptic problems. J. Sci. Comput. **49**(3), 311–331 (2011)
7. Cockburn, B., Karniadakis, G.E., Shu, C.-W. (eds.): Discontinuous Galerkin Methods. Theory, Computation and Applications. Lect. Notes Comput. Sci. Eng., vol. 11. Springer, Berlin (2000)
8. Congreve, S.: A posteriori error analysis of hp-adaptive finite element methods for second-order quasilinear PDEs. Master's thesis, University of Nottingham (2010)
9. Congreve, S.: hp–Adaptive discontinuous Galerkin finite element methods for second-order quasi-linear PDEs. PhD thesis, University of Nottingham. In preparation
10. Congreve, S., Houston, P., Wihler, T.P.: Two-grid hp-version DGFEMs for strongly monotone second–order quasilinear elliptic PDEs. In: Proceedings in Applied Mathematics and Mechanics, 82nd Annual GAMM Scientific Conference, Graz, Austria (2011)
11. Dawson, C.N., Wheeler, M.F., Woodward, C.S.: A two-grid finite difference scheme for non-linear parabolic equations. SIAM J. Numer. Anal. **35**, 435–452 (1998)
12. Gudi, T., Nataraj, N., Pani, A.K.: hp-discontinuous Galerkin methods for strongly nonlinear elliptic boundary value problems. Numer. Math. **109**, 233–268 (2008)
13. Houston, P., Robson, J., Süli, E.: Discontinuous Galerkin finite element approximation of quasilinear elliptic boundary value problems I: The scalar case. IMA J. Numer. Anal. **25**, 726–749 (2005)
14. Houston, P., Schötzau, D., Wihler, T.P.: Energy norm a posteriori error estimation of hp-adaptive discontinuous Galerkin methods for elliptic problems. Math. Models Methods Appl. Sci. **17**(1), 33–62 (2007)
15. Houston, P., Schwab, C., Süli, E.: A note on the design of hp-adaptive finite element methods for elliptic partial differential equations. Comput. Methods Appl. Mech. Eng. **194**(2–5), 229–243 (2005)
16. Houston, P., Süli, E., Wihler, T.P.: A posteriori error analysis of hp-version discontinuous Galerkin finite-element methods for second-order quasi-linear PDEs. IMA J. Numer. Anal. **28**(2), 245–273 (2007)
17. Karakashian, O.A., Pascal, F.: A posteriori error estimates for a discontinuous Galerkin approximation of second-order elliptic problems. SIAM J. Numer. Anal. **41**(6), 2374–2399 (2003)
18. Liu, W.B., Barrett, J.W.: Quasi-norm error bounds for the finite element approximation of some degenerate quasilinear elliptic equations and variational inequalities. RAIRO Modél. Math. Anal Numér. **28**(6), 725–744 (1994)
19. Marion, M., Xu, J.: Error estimates on a new nonlinear Galerkin method based on two-grid finite elements. SIAM J. Numer. Anal. **32**(4), 1170–1184 (1995)
20. Metcalf, M., Reid, J., Cohen, M.: Fortran 95/2003 Explained. Oxford University Press, Oxford (2004)
21. Ortega, J.M., Rheinboldt, W.C.: Iterative Solution of Nonlinear Equations in Several Variables. Computer Science and Applied Mathematics. Academic Press, New York (1970)
22. Ortner, C., Süli, E.: Discontinuous Galerkin finite element approximation of nonlinear second-order elliptic and hyperbolic systems. SIAM J. Numer. Anal. **45**(4), 1370–1397 (2007)
23. Saad, Y., Schultz, M.H.: GMRES: A generalized minimal residual algorithm for solving nonsymmetric linear systems. SIAM J. Sci. Stat. Comput. **7**(3), 856–869 (1986)
24. Schwab, C.: p- and hp-FEM—Theory and Applications in Solid and Fluid Mechanics. Oxford University Press, Oxford (1998)
25. Stamm, B., Wihler, T.P.: hp-optimal discontinuous Galerkin methods for linear elliptic problems. Math. Comput. **79**(272), 2117–2133 (2010)
26. Utnes, T.: Two-grid finite element formulations of the incompressible Navier–Stokes equations. Commun. Numer. Methods Eng. **13**(8), 675–684 (1997)
27. Wihler, T.P.: An hp-adaptive strategy based on continuous Sobolev embedding. J. Comput. Appl. Math. **235**, 2731–2739 (2011)
28. Wihler, T.P., Frauenfelder, P., Schwab, C.: Exponential convergence of the hp-DGFEM for diffusion problems. Comput. Math. Appl. **26**, 183–205 (2003)
29. Wu, L., Allen, M.B.: Two-grid method for mixed finite-element solution of coupled reaction-diffusion systems. Numer. Methods Partial Differ. Equ. **1999**, 589–604 (1999)
30. Xu, J.: A new class of iterative methods for nonselfadjoint or indefinite problems. SIAM J. Numer. Anal. **29**, 303–319 (1992)
31. Xu, J.: A novel two-grid method for semilinear elliptic equations. SIAM J. Sci. Comput. **15**, 231–237 (1994)
32. Xu, J.: Two-grid discretization techniques for linear and nonlinear PDEs. SIAM J. Numer. Anal. **33**, 1759–1777 (1996)
33. Zhu, L., Giani, S., Houston, P., Schötzau, D.: Energy norm a-posteriori error estimation for hp-adaptive discontinuous Galerkin methods for elliptic problems in three dimensions. Math. Model. Methods Appl. Sci. **21**(2), 267–306 (2011)